# NUMERICAL SIMULATION OF PARTICLE ADHESION DYNAMICS FOR APPLICATIONS IN NANOMEDICINE AND BIOSENSING

by

SAMAR SHAH

Presented to the Faculty of the Graduate School of
The University of Texas at Arlington in Partial Fulfillment
of the Requirements
for the Degree of

MASTER OF SCIENCE IN MECHANICAL ENGINEERING

THE UNIVERSITY OF TEXAS AT ARLINGTON

August 2009

ACKNOWLEDGEMENTS

I would like to thank my advisor, Professor Yaling Liu, for his guidance, comments, and encouragement during my research work. He taught me the value of patient and persistent work, especially when research becomes slow and frustrating. His constant enthusiasm and thorough knowledge was a great aid in my research. I would like to extend my thanks to Professor Brian Dennis and Professor Kytai Nguyen for serving on my committee.

During my Master's study at University of Texas at Arlington, I thoroughly enjoyed the courses I took, especially from Professor Wen Chan, Professor Albert Tong, Professor Seiichi Nomura, and Professor Brian Dennis. I also express my appreciation to all my lab mates for their continuous support in the lab. This acknowledgement will remain incomplete without thanking the efficient and reliable support of administrative staff of Mechanical and Aerospace Engineering Department.

Finally, I would like to express my deepest appreciation to my parents, sister and brother-in-law for their endless love and support. I also thank to my fiancée, Foram, who stood on my side providing me courage and support during my research work.

July 8, 2009

ABSTRACT

NUMERICAL SIMULATION OF PARTICLE ADHESION DYNAMICS FOR APPLICATIONS IN NANOMEDICINE AND BIOSENSING

Samar Shah, M.S.

The University of Texas at Arlington, 2009

Supervising Professor: Yaling Liu

Multifunctional nanoparticles hold considerable promise as the next generation of medicine that allow for detection of early on-set of diseases and targeted therapy with minimal toxicity. To achieve targeted drug delivery, nanoparticles are usually functionalized with certain ligands (polymers) that bind specifically to a particular type of receptors on the endothelial cell surface, which are expressed exclusively during its diseased state. The ligand coated nanoparticles, loaded with drugs inside, transport in blood stream, and adhere to diseased cells via specific adhesion. However, this whole procedure becomes complicated due to simultaneous involvement of hydrodynamic force, adhesion force and Brownian force. In particular, the ligand-receptor interaction is a sophisticated chemical process. So, the property of functionalized ligands would play a crucial role to dictate the efficiency of the targeted drug delivery by providing targeted selectivity. Similarly, the shape and dimension plays a vital role in maximizing the binding efficiency of nanocarriers. To capture nanoparticle transportation and adhesion at nanoscale, a numerical tool is developed that describes the nanoparticle motion

under vascular flow conditions. Computational modeling of targeted drug delivery via nanoparticles will offer insights to the dynamic delivery process, thus facilitate better design of nanocarriers to address the challenges of nanomedicine. The deposition process and distribution of nanoparticles under various flow rates and vascular geometry are explored.

Another aspect of this developed tool is to characterize the performance of biosensors. Nanosensors are time and cost efficient, sensitive, and enable new applications in medicine, drug discovery, and environmental monitoring. Various nanosensor platforms have been proposed, such as planar electrodes, nanowire, and nanospheres. To fully realize the potentials of the nanosensor for biomarker/nanoparticle detection, however, several key research challenges must be addressed. In particular, Nanosensors are needed for detection of low concentration biomarker such as cancer marker for early disease detection. The goal of this work is to develop an understanding of the diffusion and binding process of biomarkers under fluid flow through a novel multiscale/multiphysics computational model.

TABLE OF CONTENTS

LIST OF ILLUSTRATIONS

Figure Page

LIST OF TABLES

# CHAPTER 1

# INTRODUCTION

This thesis work consists of modeling projects in two application areas: nanomedicine and biosensor. Both applications involve modeling of brownian adhesion dynamics of functionalized nanoparticles/biomolecules onto receptor coated surface. In this chapter, the backgrounds of the two applications are addressed separately.

## 1.1 Introduction to nanomedicine

Nanomedicine defines itself as fundamental biomedical research, and is application oriented like all other biomedical research. It is one of the promising prospect by which medicine can advance. Once it reaches to the fully developed stage, it will have contributed new treatment options for better treatment of certain diseases, better imaging-techniques and early detection of disease. These will add extensively to the currently available arsenal of medicines and treatments. Over the past decade, we have witnessed mammoth research and development of nanoparticulate systems for diagnostic imaging and targeted therapeutic applications [1-7]. Various nanoplatforms, including liposomes [8, 9], polymeric micelles [10-12], quantum dots [13, 14], Au/Si/polymer shells [15-17], and dentrimers [18-20] etc. have been established with distinctive chemical compositions and biological properties. Most current nanoparticulate systems are spherical in shape. Extensive studies have been devoted to study their biological behaviors *in vitro* and *in vivo*. For example, it is known that spherical particles bigger than 200 nm are efficiently filtered by the spleen, while particles smaller than 10 nm can be quickly cleared by the kidney, thus making 10-200 nm as the ideal size range for spherical carriers. Furthermore, studies have elucidated the effects of particle size (mostly from spherical ones) on their clearance, circulation, extravasation, and distribution *in vivo*. However, effects of particle shape have been seldom studied.

## 1.2 Proposed work in nanomedicine

Nanomedicine is a well-defined application of nanotechnology in medical applications. For example, targeted drug delivery, where controlled drug dosage is administered in a patient body to treat certain disease such as Cancer. The targeted drug delivery holds very promising future because of its efficiency, perhaps reducing any risk of side effect or eliminating possible damage to surrounding healthy cells. However, one of the major hurdles and current problem in nanomedicine is to improve nanoparticle cell selectivity and adhesion efficiency through appropriate design of nanoparticles of various shapes, sizes, and materials. Similar to size, the shape of nanoparticle is a fundamental property of micro/nanoparticles that dictates their intended biological functions.

Nature has inspired us with a rich complexity of shapes at nanoscale. Among various microorganisms (e.g., bacteria, yeast), virus represents the most relevant nanoscale object in nature to artificial nanomedicine. The majority of viruses have a particle diameter between 10 and 300 nanometers [21-26]. Some filamentous viruses can have a total length of up to 1400 nm. However, their diameters are only 80 nm. Virus has a diverse collection of shapes ranging from icosahedral (a) to spherical (b, c) to bullet/rod (d, f) to filamentous (e, h), as shown in Fig. 1.1. Unlike size, the effect of particle shape is much less understood in biology. Recent data on cylindrically shaped filomicelles are beginning to reveal that non-spherical particles remarkably improved the biological properties over spherical counterpart. Despite such exciting advances, non-spherical particles haven't been widely used in nanomedicine applications due to the lack of fundamental understanding of shape effect on targeting efficiency.

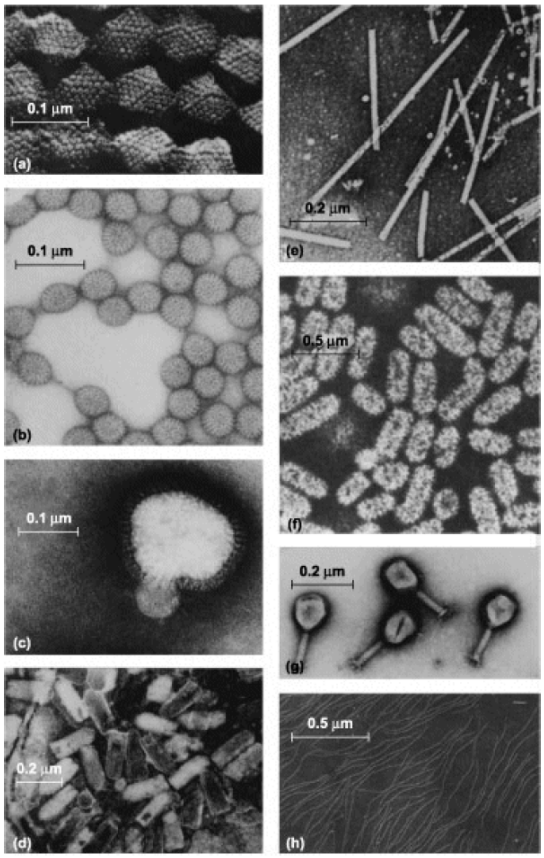


Figure 1.1 Virus nanoparticles with different shape: (a) Adenovirus (b) Rotavirus (c) Influenza virus (d) Vesicular stomatitis virus (e) Tobacco mosaic virus (f) Alfalfa mosaic virus (g) T4 bacteriophage (h) M13 bacteriophage (Adapted from: www.answers.com/topic/virus)

One of the objectives of this work is to explore the shape effect on targeted drug delivery by qualitative and quantitative numerical analysis. Recently, Geng et. al. [27] performed an *in vivo* study to determine effect of shape on circulation and demonstrated that spheres or short filomicelles are consumed by cells more easily than longer filaments. This suggests that non-spherical particle has higher chances of survival during circulation in blood vessel compare to its counter part spherical ones. Moreover, Mitragotri and coworkers have shown that the local shape of the particle at the point where a macrophage is attached, not the overall shape, dictated whether the cell began internalization [28]. These results indicate the significant advantage of controlling particle shapes in nanomedicine applications. So, this work will provide

fundamental knowledge on how shapes affect particle circulation in blood and targeting to surface receptors, which may provide biological insights on the function of viral shapes as well. In addition, it is possible to produces those different shapes of nanoparticle in the lab as shown in Fig. 1.2.

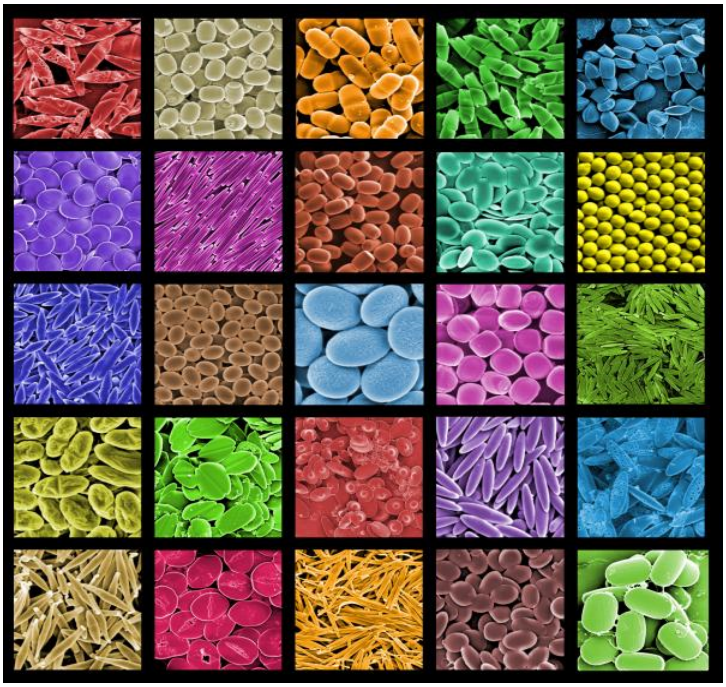

Figure 1.2 Various nanoparticles with different shapes and materials (Source: UCSB; Adapted from: http://www.sciencedaily.com/releases/2007/07/070709171558.htm).

The proposed method of this work is to uncover the shape-dependent adhesion kinetics of non-spherical nanoparticles through an unique and novel multiscale computational technique computational modeling that includes a transport-reaction model to track nanoparticle species, account for transport phenomena and define adhesion kinetic parameters for attachment and detachment process. Furthermore, adhesion/deposition process of nanoparticles under shear flow will be explored. Such process is complex due to the interplay of transport, hydrodynamic force and multivalent bond formation dynamics. The ligand-receptor binding kinetics is coupled with Brownian Dynamics to study the dynamic process of nanorods/nanodisks tumbling, diffusion and adhesion in various vascular flow conditions. This research work will result in

fundamental and in depth knowledge of shape dependent transport and targeting efficiency of nanomedicine carriers, which will provide a new guidance to the design of nanomedicine for better treatment of diseases in general.

Nanoparticles are delivered to human body by various means, oral delivery, inhalation, or injection. Among these methods commonly used method for nanoparticle drug delivery is an intravenous injection [29-31] and after injection nanoparticles transport along the blood flow. Blood itself is a complex fluid which includes red blood cell (RBC), plasma, White blood cell (WBC), etc. So, it is very likely that nanoparticles transportation will be affected by blood property as well. Blood is treated as a newtonian fluid in normal conditions, but there are certain conditions where it should be treated as a non-newtonian fluid, such as in microcirculatory flow. The main challenge of modeling blood flow with its components is to be able to incorporate physical principles into a biologically relevant model while retaining the capability to solve it numerically. For the simplicity and to focus on nanoparticle transportation/adhesion, in our modeling approach, blood is treated as a Newtonian fluid. Furthermore, transportation and distribution of nanoparticles within blood would be affected by physical interactions with blood components, in particular with RBC. For example, red blood cell collisions have been shown to enhance the diffusivity of platelets and polymer microparticles, perhaps, it causes margination of particles towards the vessel wall. In fact, nanoparticle interaction with blood components is beneficial for adhesion efficiency [32-34]. In addition, when flowing through blood, blood cells tend to concentrate towards center of the vessel, while leaving empty space to filled up with fluid and forming “cell-free” zone near to the vessel wall [35]. Thus, our focused is on modeling nanoparticle motion on micro/nano scale, assuming it has already dispersed into cell-free zone, close to the vascular wall. But, modeling of nanoparticles motion along with blood components will be a potential extension of this work. The process of nanoparticle deposition at the targeted site is divided into three distinct stages. First, the nanoparticles are marginated from the blood stream to move close to the vascular wall. The dispersion of the nanoparticles in a tube with

flow can be described by the Taylor-Aris theory [36, 37]. The diffusion process can be described by a Brownian motion, observed apparently at nanoscale. The non-spherical shape of nanoparticles adds more complexity during transportation and collision with blood components. Secondly, the interaction of nanoparticles with the vessel wall surface through ligand-receptor binding [38, 39]. The ligands on nanoparticle surface bind with receptors on vessel wall, leading to large adhesive forces. Other factors such as electrostatic, hydrodynamic, steric interactions or van der Waals (vdW) forces also lead to non-specific interactions between nanoparticle and cell membrane. However, these forces are usually several orders of magnitude smaller compared to specific adhesive force. Hence, it can be safely neglected from the present study. Finally, after initial binding, the nanoparticle may firmly adhere or may get unbound, depending on the strength of bonding, flow conditions, etc. It has been reported recently that the nanoparticle detachment is a time-dependent process with detachment probability decreases with elapsed attachment time [40].

A qualitative understanding of such dynamic deposition process experimentally is very challenging, so, a theoretical model can help to elucidate the underlying deposition mechanisms. To achieve dynamic process described as above, a 3D multiscale model of nanoparticle transport and adhesion dynamics will be established. Recently, established Immersed Finite Element Method (IFEM) for arbitrarily-shaped immersed fluid-structure interaction will be extended with adhesion kinetics to study non-spherical nanoparticle transportation, diffusion, tumbling, and adhesion [41]. At the end, the developed model will be use to characterize the influence of nanoparticle shape, size, and ligand density on adhesion probability. The deposition process and distribution of nanoparticles under various flow rates and vascular geometries will be explored.

### 1.3. Background information on Biosensors

A vast range of bio-measurements involves reaction between biomolecules in a solution and a functionalized/receptor coated surface, such as DNA microarrays [42, 43]. An important

problem in these measurements is how to perform a large number of measurements with small portions of a precious sample or how to detect biomolecules in a sample with extremely low concentration. Microfluidic system integrated with silicon-based nanosensors are considered one of the promising candidate [44]. These nanosensors are ultra sensitive to biomolecule binding due to the large surface area to volume ratio, thus enable it to detect and quantify binding of a few molecules. Researchers are investigating the potential of nanosensors to achieve rapid, ultra-sensitive, label-free detection of biomolecules at low concentration [45-49]. Bunimovich [50] reported that nanowire sensors can detect charge density change as the result of a single binding event. Morgan [51] demonstrates two ways to detect the binding of species, an indirect immunosensor, and a direct immunosensor. The indirect sensor uses a labeled element with fluorescence or luminescence after binding. The direct sensor detects the binding event through change in potential, current, resistance, mass, heat, or optical properties. Among different types of nanosensors, electrochemical sensors that translate biomolecular adsorption to change in current [52, 53] have drawn most attentions. It has been reported recently that nanowire based nanosensors can be triggered by a few binding events, thus can detect femtomolar concentration [49, 54]. It is important to design those sensors to detect target molecules with extremely low concentration within reasonable time.

### 1.4 Proposed work in characterizing performance of Biosensor

Nearly in all kind of biosensors, the focus would be to achieve best sensitivity by detecting ultra low concentration within minimal time. How to increase nanosensor sensitivity or to achieve fastest response time? A significant amount of efforts have been devoted to address this question. Sheehan et. al. [55] theoretically studied the diffusive transport of molecules toward a small sensor and claimed that sub-picomolar concentration detection using nanoscale sensors would require very long detection time (hours to days). Furthermore, they concluded that fluid flow, as high as 3.5 mm/s, marginally favors sensing with nanosensors. In contrary to their conclusion, experiments with nanowire has shown clear signal of detection in few minutes

for ~10 fM concentration solution [49, 54]. Moreover, there has been a dilemma in nanosensor community about the sensitivity of various biosensors, i.e., planar sensor, nanoelectrode, nanowire, or nanospheres. Squires et al [56] calculated the nanowire sensitivity for fM low concentration solution to be limited by a reaction limits, which indicates that even in equilibrium condition sensor can find single target molecule < 1% of the time. On other hand, planar microsensor operates neither in reaction limited nor diffusion limited regime, which suggests that micro-scale planar sensor will always have higher sensitivity compare to nanowire at ultra-low concentration. However, Nair et al. [57] reports an opposite observation from their study, which indicates at low concentration nanowire performs far better than planar sensor. In a recent work of Go et. al. [58], they explain their numerical method of detection, where they assume that out of 2000 sensors array, if as few as 5 sensors detect target molecule than they consider target molecule have been detected. While, Hahm et. al. [45] claimed that even single nanowire can always detect fM concentration within a few minutes. Thus, these contradictory studies of different group of researchers suggest that the working principles of biosensors at nanoscale are still vague and needs further investigation to predict sensor performance accurately.

Binding of biomolecules onto sensing elements, which enables detection in biosensor, is a random dynamic process. Real-time biosensors can take multiple temporal measurements of this process, thus allowing observation of the binding kinetics as well as a precise characterization of biomolecule concentration. Continuum diffusion theory has been widely used for analysis of nanosensor binding process. However, the diffusion theory breaks down at low molecular concentration < 1pM. Moreover, the continuum diffusion theory analysis does not provide stochastic error estimation for the detection process due to its continuum nature. This proposed work develops a stochastic particle model for biomolecule binding and detection process. By using different initial distributions, the error estimation can be given, which provides better solution of nanosensor detection. The developed tool will be used in the design of

nanosensor for ultra-sensitive detection of biomolecules at extremely low concentrations. The performance (i.e., sensitivity and response time) of various nanosensors will be evaluated.

# CHAPTER 2

# INTRODUCTION

## 2.1 Introduction to targeted drug delivery

In recent times, the targeted drug delivery system has become a popular idea among the researchers for the cancer treatment. The major advantage of such system is that it provides therapeutic concentration of anticancer drug at the targeted site without causing damage to the normal cells. To achieve the maximum targeting efficiency, the targeted drug delivery system should be designed optimally, especially the shape and size of nanoparticles. The drug delivery process through complex vascular environment involves dynamic interactions with the vascular surface so it will be a lengthy and tedious process to design these drug carriers through experimental studies. An appropriate method would be to develop a computational modeling technique, which incorporates fundamental physical principles that dictates dynamics of nanoparticle delivery and adhesion process. The computational tool provides insights of the delivery process and the interaction of nanoparticle with the cells. Quantitative analysis based on the developed model will facilitate an optimum model of the drug delivery system to the researchers and support a rational framework for the cancer treatment research.

Nanoparticles usually enter the vascular circulation stream through intravenous injection [29-31]. The targeted delivery efficiency is directly related to the nanoparticle selectively and ability to bind at the targeted site. Though highly selective nanoparticles have reduced binding probability in non-target regions, the majority of nanoparticles are still lost in the vascular network due to non-specific adhesion. It is thus important to predict the lost of nanoparticles in the up-stream and the nanoparticle concentration when it reaches the targeted

region. A multiscale framework is pursued to model the targeted drug delivery systems, as shown in Fig. 2.1.

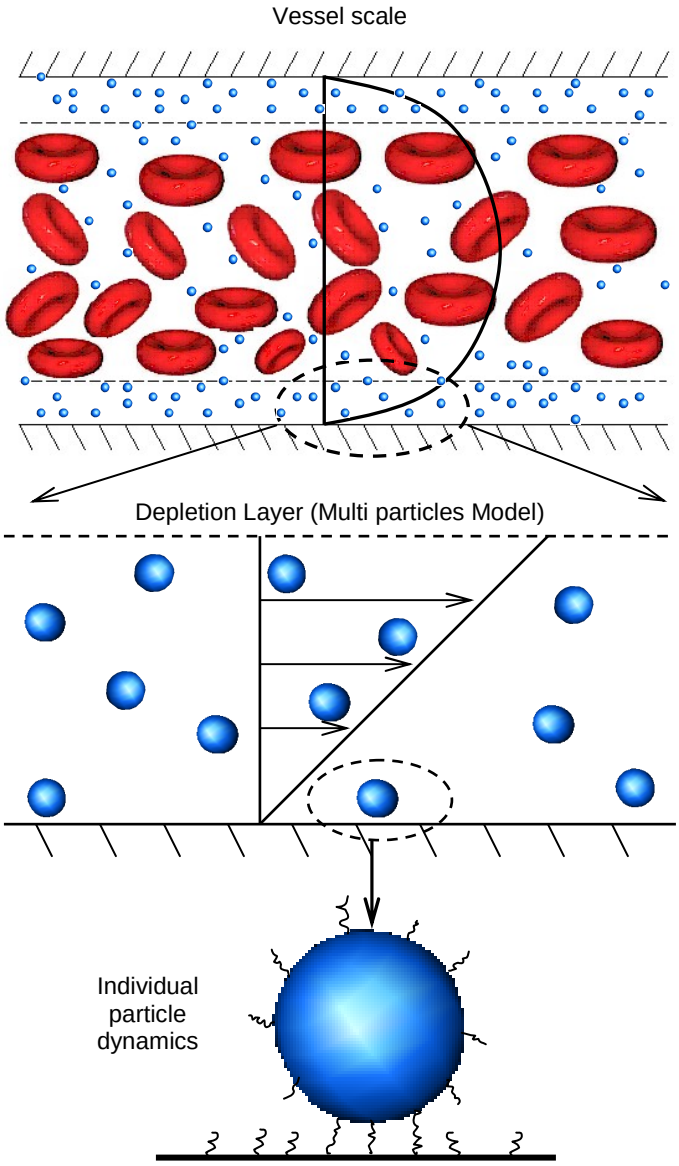


Figure 2.1 Multiscale model of the targeted drug delivery.

The vessel scale involves interaction between nanoparticles and the blood components. Due to the limitation of capability of current model, this is not a part of current work, but it is considered as a potential future work. Moreover, the focus of this work is to explore an optimum

design of nanoparticle near to the target region, where the effect of nanoparticle shape on binding probability becomes more apparent. The significance of the depletion layer will be discussed in section 2.4.

## 2.2 Fundamental theories of targeted drug delivery

Theoretical modeling of nanoparticle adhesion dynamics has been focused mostly on spherical particles [59-61]. It is only recently that non-spherical nanoparticle attracts some attention. For example, Decuzzi and Ferrari [59, 62, 63] have studied the margination of nanoparticle vector in blood stream, where the dispersion of nanoparticles in a newtonian fluid is investigated. The same group of authors has also studied the adhesion probability of different shaped nanoparticles and has showed that oblate-shaped nanoparticles can considerably increase adhesion probability to the cellular receptors than spherical particles of the same volume. However, their model considers an equilibrium configuration and in reality, adhesion process is a dynamic process, thus an equilibrium model is unable to capture dynamic adhesion process. Also, in their work, the margination and adhesion process are studied separately. A coupled model that links margination with adhesion dynamics and applicable to nanoparticle of various shapes is yet to be developed. Moreover, the deposition and spatial distribution of nanoparticles in different blood vessel geometries are not studied at all, a major hurdle to compare simulation results directly with *in vitro* or *vivo* measurements.

To address these imitations, an integrated model that couples the dynamic diffusion and tumbling motion together with nanoparticle adhesion dynamics is developed. Regardless of the potential mechanism that may affect drug delivery, a very recent computer simulation in two spatial dimensions have demonstrated that nanoscale drug delivery systems could in principle be affected by similar limitations as traditional chemotherapy. Nanoparticles first have to be transported in the blood stream to the vicinity of the tumor and extravagate from the blood vessels into the interstitial space; then the drug needs to be released and diffuse through or around the tumor cells [34].

There are two binding mechanisms for nanoparticles to adhere at any vascular site: specific and non-specific binding. Targeted drug delivery is achieved via specific adhesion, where, nanoparticles are functionalized with polymers that bind specifically to a particular type of receptors on the cell surface; these receptors are exclusively expressed during certain disease state. The commonly used ligands include small organic molecules (e.g. folic acid), peptides (cyclic RGD), antibody, or DNA/RNA aptamers. Besides specific adhesion, other factors such as electrostatic, hydrodynamic, steric interactions or van der Waals (vdW) forces lead to non-specific interactions between nanoparticle and cell membrane. Although non-specific binding force is usually orders of magnitude smaller compared to specific adhesive force, significant amount of nanoparticles are deposited non-specifically along the long vascular pathway before it reaches the target region, leading to toxic effects on healthy tissue, inadequate targeting, and impaired transport to the tumor site. Thus, it is very critical to design and functionalize nanoparticle in a systematic manner to avoid damage to healthy cells due to non-specific adhesion.

Particulate Brownian adhesion dynamics model is used to capture the nanoparticle adhesion process over the vascular surface. The ligand-receptor adhesion kinetics is integrated into the Brownian dynamics model to describe the transportation, diffusion, and adhesion of arbitrarily shaped particles. This model is then integrated in immersed finite element method (IFEM) to obtain quantitive results of nanoparticle binding probability under vascular flow condition. Although IFEM is an essential part of this modeling work, theoretical aspects of IFEM, which is already developed, isn't covered in this work but reader can find details in references [64, 65].

IFEM can be used for fully coupled fluid-structure interaction problems, i.e., solving particle motion in a fluid while capturing the influence of nanoparticle on fluid flow. However, due to Brownian motion, it is computationally very expensive to calculate the change of fluid flow due to nanoparticle motion at each time step. Since effect of nanoparticle motion is limited

locally, we neglect the influence of nanoparticle motion on fluid flow and focus on the nanoparticle motion and adhesion under fluid flow. Moreover, although IFEM can handle deformable particles immersed in a fluid; the nanoparticles are treated as rigid bodies in this work since focus is on nanoparticle shape effect on adhesion process. The nanoparticle compliance will be the topic of future studies.

*2.2.1. Adhesion Kinetics of nanoparticle*

The ligand-receptor binding is described as a bond reaction process. When a nanoparticle approaches the vascular wall, ligands on the nanoparticle surface form bonds with receptors on the vascular wall, as demonstrated in Fig. 2.2.

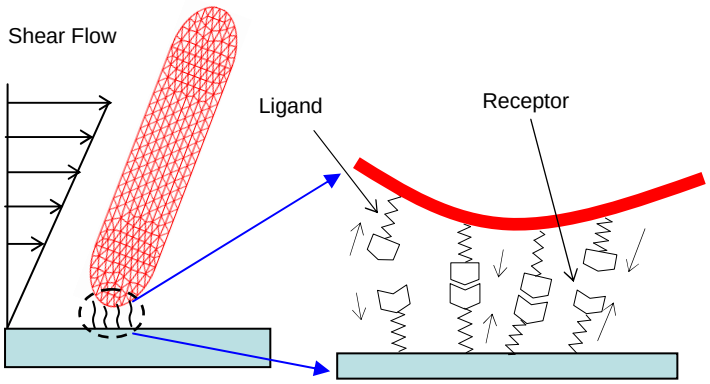


Figure 2.2 Model of ligand-receptor binding kinetics between ligand-coated nanoparticle surface and receptor coated vascular wall surface.

An adhesion kinetic equation is used to calculate the bond density $N_b$ [38] and the rate of bond formation is given by:

$$\frac{\partial N_b}{\partial t} = k_f (N_l - N_b)(N_r - N_b) - k_r N_b \qquad (2.1)$$

Where, $N_l$ and $N_r$ are the ligand and receptor densities, respectively; $k_r$ and $k_f$ are the reverse and forward reaction rates, respectively. This reaction model represents a conservation equation of the different species (ligands, receptors, and bonds). $k_r$ and $k_f$ are functions of bond lengths:

$$k_r = k_r^0 \exp\left(-(\sigma - k_{ts})L^2 / 2B_z\right) \quad (2.2)$$

$$k_f = k_f^0 \exp\left(-k_{ts}L^2 / 2B_z\right) \quad (2.3)$$

Where, $\sigma$ is the bond elastic constant; $k_{ts}$ is the bond elastic constant at transient state; $B_z$ is thermal energy; $k_r^0$ and $k_f^0$ are the reverse and forward reaction rates at zero load of ligand-receptor pair, respectively; $L$ is the difference of bond length y and equilibrium length $\lambda$. The physical parameters are mentioned in the Table 2.1.

Table 2.1 List of physical parameters

| **Definition** | **Symbol** | **Value** | **Reference** |
|---|---|---|---|
| Ligand Density | $N_l$ | 2.0 x $10^{10}$ (sites/cm$^2$) | Lawrence and Springer (1991)[66] |
| Receptor Density | $N_r$ | 2.0 -5.0 x $10^{10}$ (sites/cm$^2$) | Bell et al. (1984)[67] |
| Reverse reaction rate | $k_r$ | 0.5 (1/s) | Bell (1978)[68] |
| Forward reaction rate | $k_f$ | 1.0 x $10^{-9}$ (cm$^2$/s) | Bell (1978) [68] |
| Equilibrium bond length | $\lambda$ | 20 nm | Bell (1978)[68] |
| Static bond spring constant | $\sigma$ | 0.5 (dyne/cm) | Dembo et al. (1988)[38] |
| Transient bond elastic constant | $k_{ts}$ | 0.48 (dyne/cm) | Dembo et al. (1988)[38] |
| Thermal Energy | $B_z$ | 4.0 x $10^{-14}$ (erg) | Dembo et al. (1988)[38] |
| Fluid viscosity | $\mu$ | 0.01 (g/cm-s) | - |

The receptor-ligand bonds are modeled as springs with spring constant $\sigma$ and equilibrium length $\lambda$, thus the bond forces are described as a function of bond length $y$. Then, the ligand-receptor bond forces can be accumulated on finite element surface through integration over the nanoparticle surface. Equations of bond forces and integrated adhesion forces are given as [69]:

$$f_L = \sigma(y - \lambda) \tag{2.4}$$

$$\sigma^S \cdot n = \int N_b \; f_L \, (X^c) \, d\Gamma \tag{2.5}$$

Such, adhesion force is coupled with the fluid-structure interaction force in the IFEM formulation. Similar, adhesion model has been used by Chang et al. [70] and Dong et al. [39] in the study of white blood cell rolling.

*2.2.2. Brownian Dynamics*

Fundamental theories of Brownian dynamics indicates the impacts of random collisions from surrounding liquid molecules on motion of a immersed small particle [71-73]. The influence of Brownian motion on behavior of platelets and blood cells in blood flow has been studied extensively [74-76]. Patankar et al. [77] have proposed an algorithm for direct numerical simulation of Brownian motion by adding random disturbance in fluids. At microscale, the drag force acting on particles such as blood cells is significantly large (> 50 pN for particle size > 1 μm) compare to Brownian force, thus Brownian motion is negligible [74]. While, at nanoscale Brownian force becomes a dominant force to drive nanoparticle under vascular flow or near to the vascular wall surface, where, the drag force acting on a nanoparticle is relatively small. Due to Brownian motion, a nanoparticle may diffuse towards the wall surface, as it reaches close enough to the receptor coated vascular wall surface, the bond formation is initiated. The random forces ***R(t)*** and torque ***T(t)*** acting on a nanoparticle is responsible for Brownian motion and rotation and satisfy the second fluctuation-dissipation theorem [78]:

$$\left\langle \mathbf{R}_i(t) \right\rangle = 0 \,, \; \left\langle \mathbf{T}_i(t) \right\rangle = 0 \tag{2.6}$$

$$\left\langle \mathbf{R}_i(t) \mathbf{R}_j(t') \right\rangle = 2 \; k_B T \beta_t \, \delta_{ij} \, \delta(t - t') \, \boldsymbol{\delta} \tag{2.7}$$

$$\left\langle \mathbf{T}_i(t) \mathbf{T}_j(t') \right\rangle = 2 \; k_B T \beta_r \, \delta_{ij} \, \delta(t - t') \, \boldsymbol{\delta} \tag{2.8}$$

Where, δ is the unit-second order tensor, $\delta_{ij}$ is the Kronecker delta, δ (t – t') is the Dirac delta function, $k_B T$ is thermal energy of system, $\beta_t$ and $\beta_r$ are the translational and rotational friction coefficient of nanoparticle, respectively.

Friction coefficients depend on several physical parameters, such as fluid viscosity, size and shape of the nanoparticle. The friction coefficient for spherical-shaped particles can be easily derived from Stokes' law. However, there is no empirical formula available for friction coefficient of arbitrarily-shaped particles. In literature [79-81], there are empirical formulas for friction coefficients of oblate or rod-shaped particle, but those are limited to only few shapes. So, the aim of this work is to develop a versatile model that can handle any arbitrary shape particle as well. To model dynamic translation and rotation of arbitrarily-shaped particles, a methodology similar to Tran-Cong et. al [81] is adopted. An arbitrarily-shaped particle is discretized into finite elements. Each element is considered effectively as a small sphere whose volume is equivalent that of the element. At the end, friction coefficient of the whole particle is a summation of the friction coefficient of discretized elements:

$$\beta_t = \frac{\sum_{i=1}^{n} \beta_{t,i} \cdot v_i}{V} = \frac{\sum_{i=1}^{n} 3\pi \mu d_i \cdot v_i}{V} \tag{2.9}$$

$$\beta_r = \frac{\sum_{i=1}^{n} \beta_{r,i} \cdot \omega_i}{\omega} = \frac{\sum_{i=1}^{n} \pi \mu d_i^{\,3} \cdot \omega_i}{\omega} \tag{2.10}$$

Where, $\mu$ is fluid viscosity, $d_i$ is an effective diameter of $i^{th}$ element, $\beta_i$ is friction coefficient of small sphere, $v_i$ and $V$ are the local and average velocity difference of nanoparticle and fluid field, $\omega_i$ and $\omega$ are the local and average angular velocity difference of nanoparticle and fluid field, respectively. In real implementation, since the friction coefficient changes with the relative orientation of the particle with flow direction, an orientation factor is multiplied with friction coefficients to project the particle normal to the flow direction.

The velocity of a particle moving under a deterministic force in a fluid with velocity $V_f$, is given by:

$$\mathbf{V}_s = \left( \frac{\mathbf{F}_{\text{deter}}}{\beta_{\text{particle}}} + \mathbf{V}_f \right) \cdot \left( 1 - e^{-\frac{\beta_t}{m} \cdot t} \right) \tag{2.11}$$

Where, $F_{deter}$ is the total deterministic forces acting on the nanoparticle (Brownian force, adhesion force, etc.), $V_s$ and $V_f$ are solid and fluid velocity, respectively. For a time step much greater than characteristic time constant $(m/\beta_t)$, the nanoparticle moves with a terminal velocity and Eq. (2.11) reduces to:

$$\mathbf{V}_s = \frac{\mathbf{F}_{\text{deter}}}{\beta_t} + \mathbf{V}_f \tag{2.12}$$

By implementing this approach, we assume that deterministic force acting on the particle is balanced by the drag force from the fluid. This is a reasonable assumption since the mass of a nanoparticle is so small and that inertia effect can be neglected. This terminal velocity is use to update the nanoparticle position in translation direction. Similarly, the angular velocity of nanoparticle can be obtained through:

$$\boldsymbol{\omega}_s = \frac{\mathbf{T}_{\text{deter}}}{\beta_r} + \boldsymbol{\omega}_f \tag{2.13}$$

Where, $\omega_f$ is the angular velocity due to fluid flow. Using this translational and angular velocity, particle nodal positions are updated based on its distance from the center of the particle as:

$$\mathbf{v}_i = \mathbf{V}_s + \boldsymbol{\omega} \times \mathbf{r}_i \tag{2.14}$$

Incompressible viscous fluid flow is solved by the Navier–Stokes equations:

$$\rho\left(\frac{\partial \mathbf{v}_f}{\partial t} + \mathbf{v}_f \cdot \nabla \mathbf{v}_f\right) = -\nabla p + \mu \nabla^2 \mathbf{v}_f \tag{2.15}$$

$$\nabla \cdot \mathbf{v}_f = 0 \tag{2.16}$$

To eliminate any numerical oscillations, the velocity test function is employed along with the stabilization parameters. Using integration by parts and the divergence theorem, the Patrov-Galarkin weak form is obtained. Then, the non-linear system is solved using the Newton-Raphson method. Moreover, the Generalized Minimum Residual (GMRES) iterative algorithm is

employed to improve computation efficiency and to compute residuals based on matrix-free techniques [82]. The details of the derivation and implementation can be referred to [64, 65].

## 2.3 Nanoparticle Adhesion Probability Model

### *2.3.1. Theoretical adhesion probability model*

A numerical model is built based on the previous work by Decuzzi and Ferrari [60, 62] to describe the cell targeting processes of nanorods and nanodisks under flow conditions. The adhesion probability $P_a$ is characterized by the probabilistic kinetic formulation of McQuarrie [83]:

$$P_a \; ; \; m_r m_l K_a^o A_c \exp\left[-\frac{\lambda f}{k_B T}\right] \tag{2.17}$$

Where, $m_r$ is receptor density on the substrate surface, $m_l$ is ligand density on particle surface, $A_c$ is contact area of particle, $f$ is force acting per unit ligand-receptor pair, $k_BT$ is thermal energy of system, $\lambda$ is a characteristic length of ligand-receptor bond, and $K_a^o$ is the affinity constant of ligand-receptor pair at zero load. Further, $f$ can be expressed by following equation:

$$f = F_{dis} \Big/ A_c = F \Big/ A_c + 2T \Big/ (A_c r_o) \tag{2.18}$$

Where, $F_{dis}$ is the dislodging force due to hydrodynamic forces, comprised of two components, drag force along the flow direction $F = 6\pi a l \mu S F^s$ and torque $T = 4\pi a^3 \mu S T^s$. The contact area of the particle $A_c$ is a surface area of the spheroid below a separation distance $h_o$ from the wall surface. It can be approximated as following:

$$A_c \cong \pi r_o^2 = \pi a^2 \left[1 - \left(1 - \frac{h_o - \delta_{eq}}{a}\gamma\right)^2\right] \tag{2.19}$$

Where, $a$ is a major radius of the particle, $\delta_{eq}$ is an equilibrium separation distance between the particle and wall surface, and $\gamma$ is an aspect ratio of the particle. The details of the formulation and the constants used in the model can be found in a reference [84]. It is evident

from the equation (2.17) that the probability of adhesion is proportional to the term $m_l.m_l.K_a^o$. However, the focus is on studying the effect of particle volume and the aspect ratio on the adhesion probability. Thus, the equation(2.17) is normalized by dividing both the sides with the term $m_l.m_l.K_a^o$ to eliminate its effect.

Normalized adhesion probability of oblate-, rod- and disc-shaped nanoparticles for a wall shear stress of 1 Pascal is plotted as a function of particle volume in Fig. 2.3. The aspect ratio of disc (diameter over height) and rod (length over diameter) are chosen to be 5.

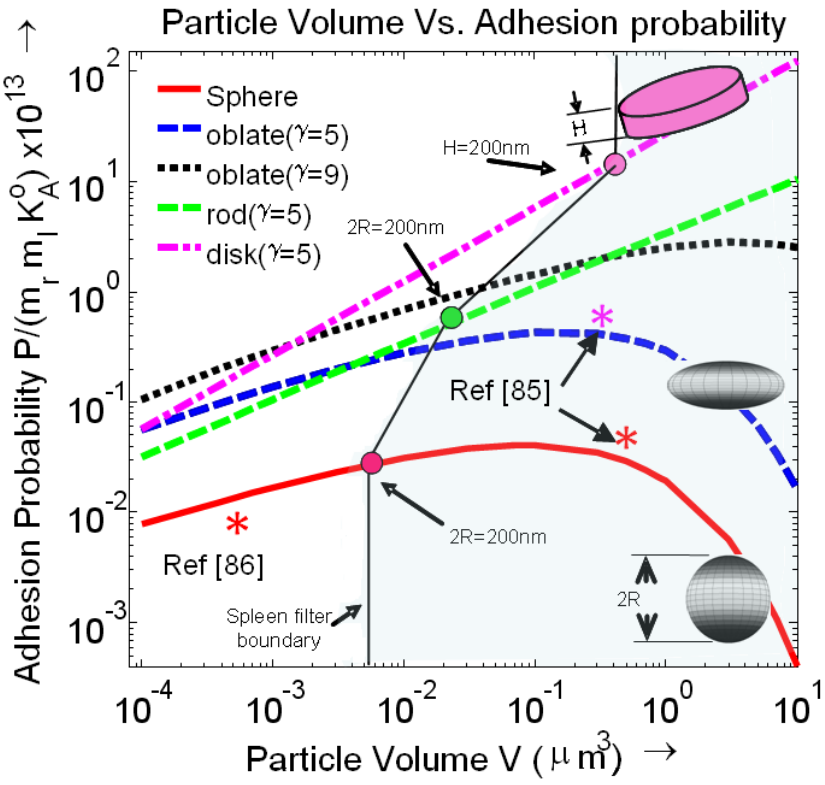


Figure 2.3 Adhesion probabilities of nanoparticles of various shapes as a function of particle volume, γ is the aspect ratio. [85, 86]

As shown in Fig. 2.3, when the particle volume increases, the adhesion probability increases first and then decreases for the spherical particle. With increase in particle volume, larger surface area is available for the bond formation, but after certain critical volume due to the large volume, $F_{dis}$ becomes dominant factor and it further reduces the probability of

adhesion. While for oblate-, disc- and rod-shaped particles, this critical volume is comparatively large (out of the plot range). Due the shape effect, the critical volume of the non-spherical particles shifts to the right side of the plot. For the volume range considered, the oblate, rod and disc particles show remarkably higher adhesion probabilities than the spherical particles of the same volume. To further reveal the biological relevance of the data, particle volumes with 200 nm in at least one dimension representing the spleen filtration threshold is indicated as lines in Fig. 2.3. Particles bigger than the spleen filtering boundary volumes (blue zone in Fig. 2.3) cannot pass through the spleen. This suggests that particle volumes should be below the spleen filtering boundary volumes for the targeted drug delivery application. Furthermore, the disc-shaped nanoparticles represent the highest adhesion probability and the largest volume to be pass through the spleen, resulting in a 300 times higher efficacy for cell targeting and 40 times higher drug-loading capability than the spherical counterpart. The adhesion probability of the rod particle, with the aspect ratio of 5, is about 20 times higher than the spherical particle. Similarly, the oblate shaped nanoparticles exhibit almost 10 times higher adhesion probability compare to the spherical particles over the entire range of volume considered. The predicted adhesion probability agrees with the limited available experimental data in literature [85, 86] as marked on Fig. 2.3. These preliminary results strongly support the key hypothesis of this work and motivate to investigate the effect of particle shapes/size on targeted drug delivery.

*2.3.2. Effect of shear rate on dissociation probability of nanoparticles*

Once, the adhesion probability is derived from the equation of probabilistic formulation(2.17), the dissociations probability ($P_d$) can be easily calculated as 1-*Pa*. The dissociation probability is normalized by a factor, dissociation probability at zero shear rates. This defines the dissociation probability range from 0 to 1. The normalized dissociation probability ($P_d$) of nanorod and nanosphere under different shear rates is plotted in Fig. 2.4.

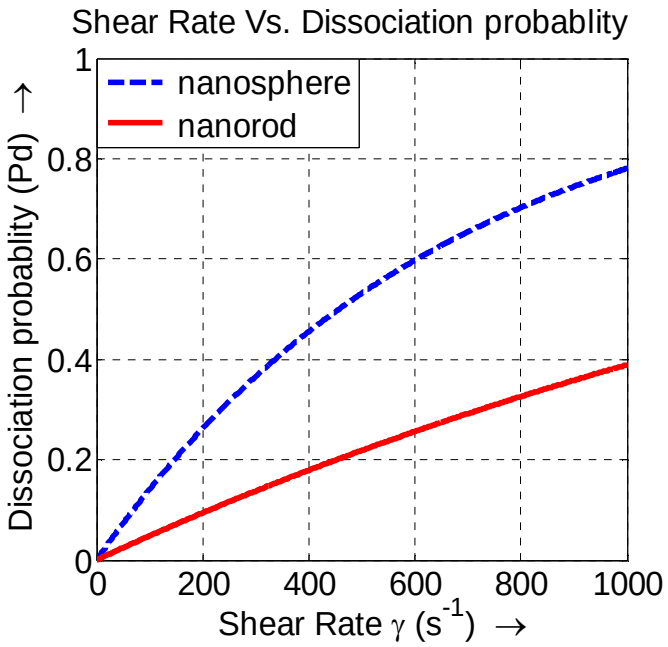


Figure 2.4 Particle dissociation probabilities as a function of shear rate for nanorod and nanosphere. The dissociation probability is normalized with zero shear rate.

Nanosphere of radius of 100 nm is considered, while nanorod of the same radius but with aspect ratio of 5 is considered. Increase in magnitude of shear rate cause ascend in shear/dislodging force which increases the dissociation probability. Further, for a given shear rate the dissociation probability of a nanorod is significantly less as compared to a nanosphere, since the former has larger surface area available for binding. While an analytical expression can be derived for the dissociation probability of nanosphere or nanorod, the binding probability is much more complex and needs to be obtained numerically due to the dynamic binding process, where the configuration of nanoparticle changes constantly under deterministic forces and that will be discussed in next sections of this chapter.

## 2.4 Simulation results on nanoparticle dynamics

There are numerous physical factors that impact nanoparticle interaction with the vascular wall surface under vascular flow condition, such as nanoparticle-wall distance,

nanoparticle shape, ligand density, shear rate etc. The influences of nanoparticle shape, ligand density, and shear rates on adhesion kinetics is studied through simulation results.

The theoretical [87] and experimental [88] efforts have revealed that while blood flows through small vessels, there is cell-free plasma layer near to wall and a core region of suspension of all the erythrocytes (blood cells). This two-phase model is treated as two fluid layers with different viscosities, mainly due to variation in percentage of hematocrit [89, 90]. Nair et al.[91] used a two-phase model for the blood in modeling transport of oxygen in the arterioles. In their model, they considered a cell-rich core surrounded by a cell-free plasma layer. Pralhad et. al.[92] used a two-fluid model of polar fluid to analyze the flow of blood through stenotic arteries. To initiate bond formation, nanoparticles must stay very close to the wall, inside the so call depletion layer/cell-free zone, a near-wall region [35], as shown in Fig. 2.1. The thickness of the depletion layer is found to be varying from 2-5 μm, independent of vessel size for vessels with diameter above 20 μm [93-95]. This suggests that binding probabilities of nanoparticles should be studied for a range of layer thicknesses.

Dispersion of nanoparticles near to the depletion layer surface can be evaluated using a continuum model. The advantage of a continuum model is that it can effectively handle a large vascular network without much computational burden. However, it is unable to explore the adhesion process of individual nanoparticles, and it lacks in providing quantitative analysis of the drug delivery process. To demonstrate the capability of developed tool, multiple particles model have been developed (section 2.5), which can handle about ~1000 particles in a system. The following sections 2.4.1 and 2.4.2 demonstrate influence of shape and ligand density on nanoparticle adhesion kinetics. The details of mesh and dimensions of nanoparticle and channel used can be found in appendix A.

*2.4.1. Influence of shape on nanoparticle adhesion kinetics*

To test the influence of nanoparticle shape on adhesion kinetics, two nanoparticles of different shapes, spherical and non–spherical, but of the same volumes are considered. In the

simulation, a spherical particle and rod-shaped particle are initially positioned with their center 600 nm above a receptor-coated surface, as shown in Fig. 2.5.

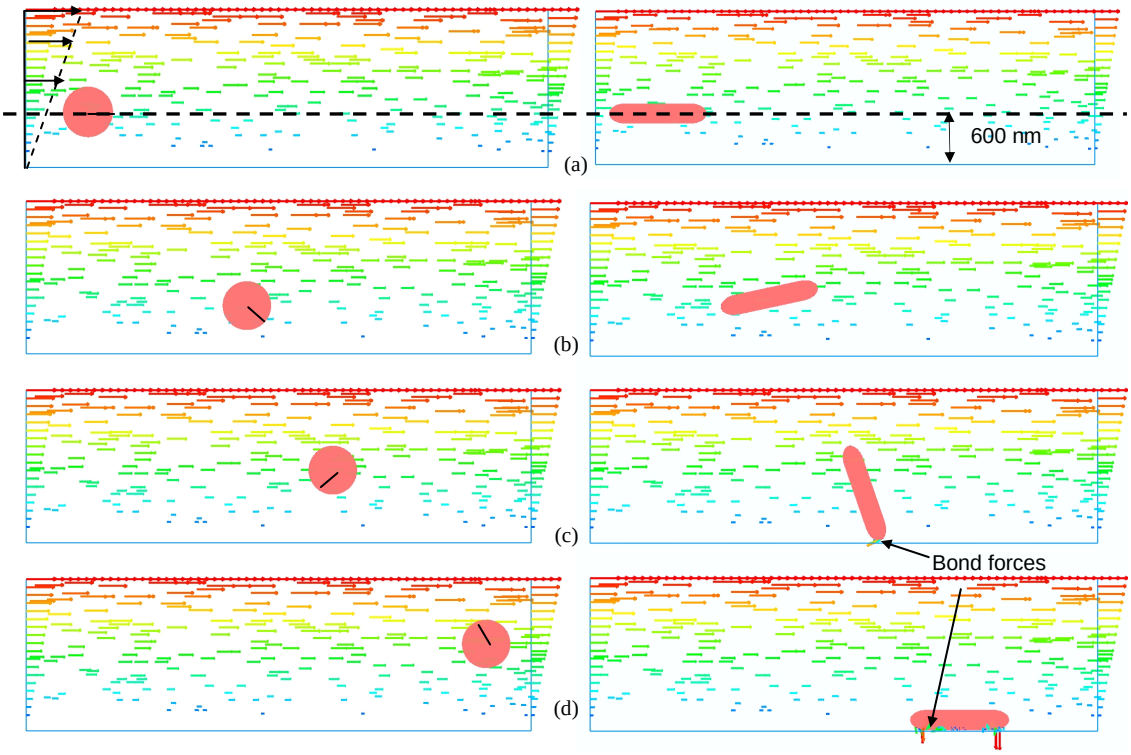


Figure 2.5 The shape dependent adhesion kinetics. The left column shows a spherical particle flow away without contact with surface; the right column shows a nanorod tumbles and gets deposited. (a), (b), (c), (d) are at time t=0 s, 0.25 s, 0.5s, and 0.75 s, respectively. The line on the spherical particle indicates its rotation (for dimensions refer to A.1).

The shear velocity is applied at the top of channel to generate a shear rate of $8.0s^{-1}$. Nanoparticles are allowed to move freely through the channel under influence of shear flow and Brownian force. However, it fails to make any contact or interaction with the vessel wall. Although, Brownian motion is incorporated in the model, but for a given velocity and a channel length, the diffusion length isn't large enough to make the spherical particle to reach close enough to the wall surface, required to initialize bonding. Due to the non-spherical shape, rod particle exhibits the tumbling motion while flowing through the channel. Thus, during such tumbling motion, the rod-shaped particle contacts with the receptor coated wall with bonds formed at the long axis end first. Then under steadily growing adhesion force, nanoparticle

firmly adheres to the vessel wall at its equilibrium state. Though, the simulation result is just for one trial and doesn't provide any quantitative data, but it is able to capture performance difference of two different shaped nanoparticles.

*2.4.2. Effect of ligand density on nanoparticle adhesion kinetics*

Besides the shape, ligand density also largely influences nanoparticle adhesion kinetics. To investigate the effect of ligand density on nanoparticle adhesion kinetics, the deposition process of two nanorods is compared under same physical flow condition. Again, a shear rate of $8.0s^{-1}$ is generated within the channel, as shown in Fig. 2.6.

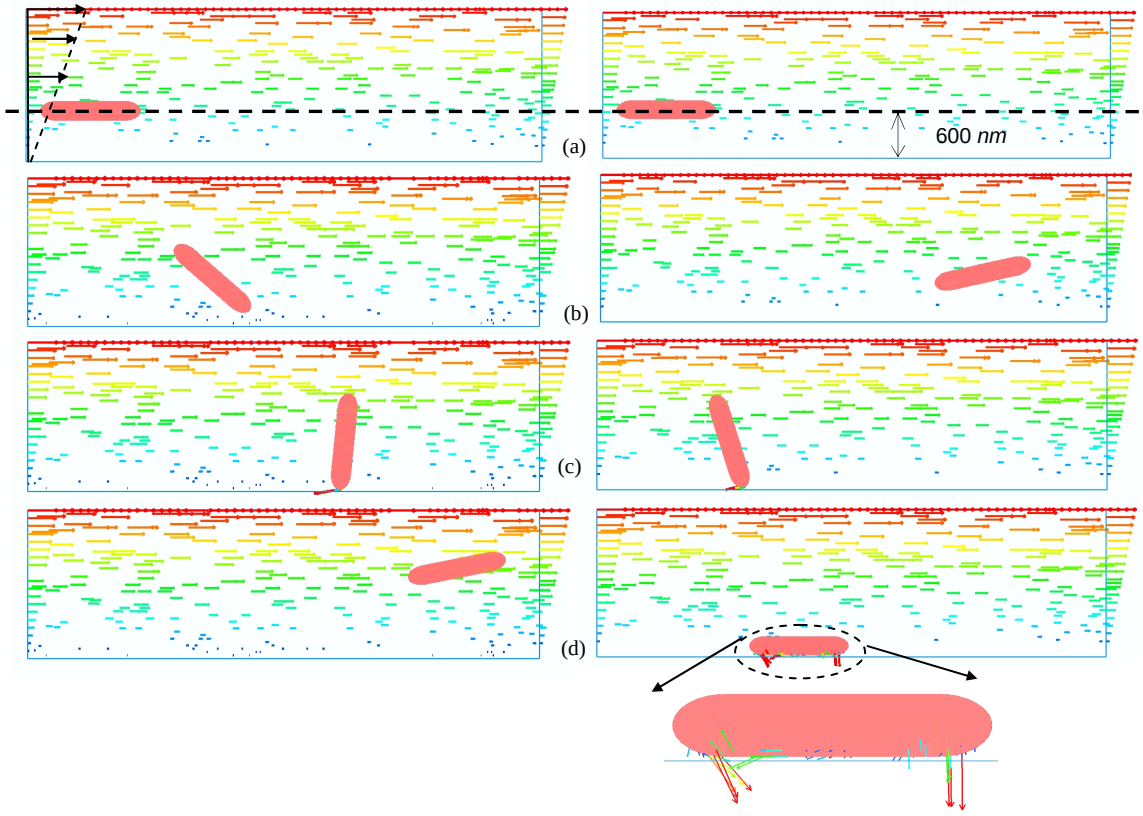


Figure 2.6 Influence of ligand density on adhesion kinetics. The left column and right column has a nanorod with low and high ligand coating respectively; A, B, C, D are at t=0 s, 0.25 s, 0.5s, and 0.75 s.

Nanorods are coated with a ligand density of $410\mu m^{-2}$ and $3400\mu m^{-2}$, respectively. The corresponding number of ligands on each particle is 15 and 120, respectively. The significance

of ligand density is that larger the density stronger/faster the bond formation is. As shown in Fig. 2.6, the nanorod with low ligand density contacts with the wall surface at its end during tumbling motion, still it gets unbounded due to weak adhesion force. Thus, the limited numbers of ligands on the surface are unable to hold the nanoparticle at the contact site. In comparison, the nanorod with high ligand density firmly adheres upon initial contact as a result of multivalent bond formation. Therefore, the large number of bond sites ensures firm adhesion of nanorod at the contact site.

*2.4.3. Statistical variance of nanoparticle trajectory*

Nanorods are expected to have a higher probability to contact with the wall surface than their spherical counter parts because of tumbling motion. To test this hypothesis, trajectories of spherical and non-spherical nanoparticles under the same flow condition are compared. A hear rate of $8.0s^{-1}$ is employed for the both cases. The simulations are carried over the channel with the length equal to 15 µm and the height equal to 5 µm.

To illustrate the fluctuations of nanoparticle-wall distance, minimum distance between the nanoparticle surface and the wall surface is recorded over the time, as shown in Fig. 2.7 (a). Such nanoparticle trajectory indicates the path of nanoparticle during its motion through the channel.

In a series of simulation runs, a nanosphere and a nanorod are placed initially 650 nm above the wall surface. The trajectories of nanorod and nanosphere of 20 independent simulations are plotted in Fig.2.7 (b).

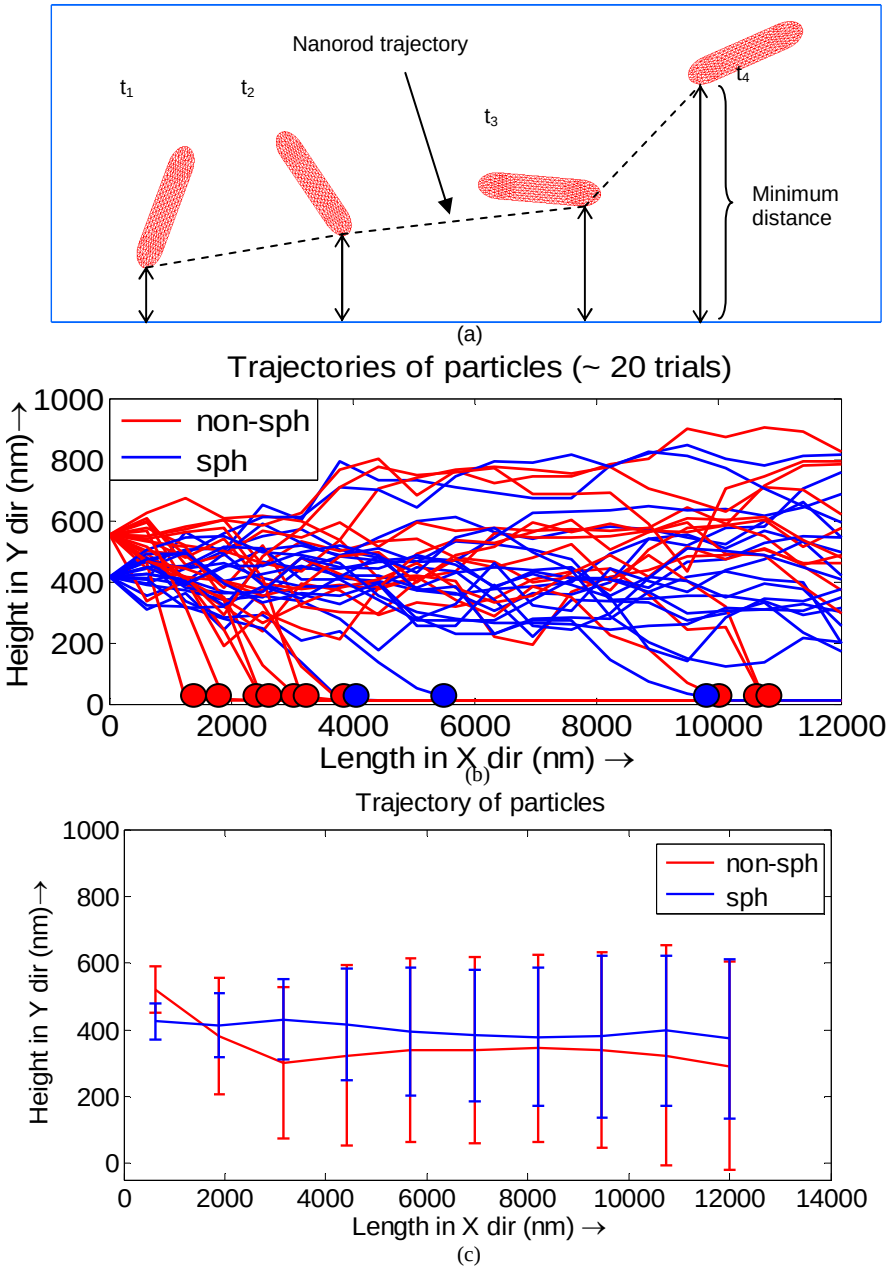


Figure 2.7 Comparing trajectories of nanorod and nanosphere to study shape effect on particle adhesion dynamics. (a) Illustration of measurement of minimum distance between nanoparticle and wall surface at different times. (b) Trajectories of 20 trials of nanorod and nanosphere, where red spot indicates adhesion of nanorod and blue spot indicates adhesion of nanosphere at that location (c) Mean trajectory of 20 trials of nanorod and nanosphere with standard deviation shown as vertical bar.

The simulation result elucidates that a nanorod has larger fluctuations in trajectories due to tumbling motion, thus it has more contact/adhesion events compared to that of nanosphere, as shown in Fig. 2.7 (c). Moreover, in a fixed number of trials, ten nanorods are deposited while only three nanospheres are deposited. Probability of spherical particle to contact with wall surface solely depends on brownian diffusion; while in case of nanorod, probability of contact is enhanced by tumbling motion. Thus, this result supports hypothesis of this work that nanorod has higher contact probability than the nanosphere for given physical condition.

*2.4.4. Effect of depletion layer thickness on binding probability*

The focus of this simulation study is to characterize the binding probability of nanoparticles under vascular conditions for a given depletion layer thickness. The theoretical model has shown that adhesion probability is influenced by several parameters such as ligand density, nanoparticle shape and size, vascular flow condition, etc. The effect of ligand density on nanoparticle adhesion dynamics is already been shown qualitatively. However, actual targeting process is a dynamic process, involving transportation and diffusion process. This suggests the need of another parameter namely, binding probability, which effectively represents the binding probability of nanoparticle from a certain distance of the wall surface. It is the binding probability that actually dictates how many nanoparticles will actually bind to the surface among the number of nanoparticles present within the cell free zone. This study is dedicated on studying the effect of two parameters, the channel height and the shear rate, on nanoparticle binding probability. To ensure consistency and to study sole effect of mentioned parameters among all the cases, the rest of the parameters are kept constant. For example, the value of ligand density is sufficiently high to guarantee firm adhesion of nanoparticles (typically, adhesion force varies from 1 pN – 100 pN, while detachment forces are limited 0.01 pN). Moreover, in a recent study, it has been shown that once nanoparticle tether to the receptor coated surface, it is very unlikely that nanoparticle gets detached under hydrodynamics force

[40]. As a consequence this section is focusing on determining binding probability of nanoparticles rather than adhesion probability. The mesh information, nanoparticle and channel dimensions are mentioned in appendix (A.2). The simulation parameters are listed in table. 1, unless otherwise noted.

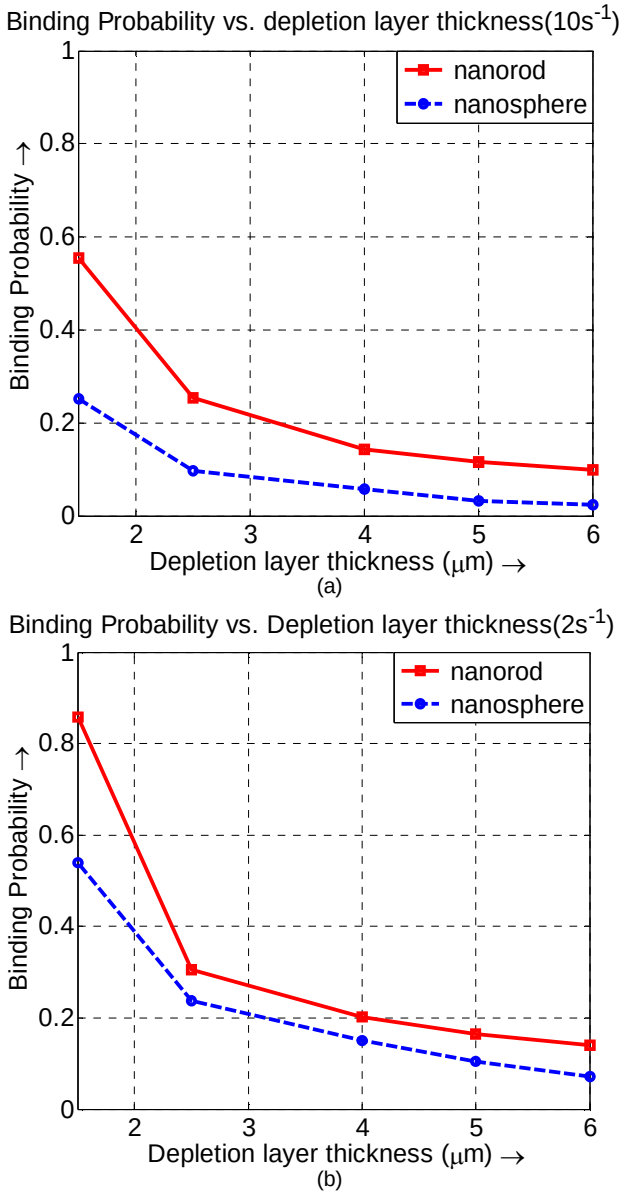


Figure 2.8 Studying effect of depletion layer thickness on binding probability of nanorods and nanosphere. (a) For shear rate of $2s^{-1}$, binding probability of nanorod and nanosphere is shown. (b) For shear rate of $10s^{-1}$, binding probability of nanorod and nanosphere is shown.

The simulation begins with randomly assigned initial positions of nanoparticle at the channel inlet. The nanoparticle transportation is described by Brownian adhesion dynamics model. To ensure statistical accuracy, binding probability is evaluated based on the results of ~ 200 independent trials. The number of bonded nanoparticles is counted and normalized by the total number of nanoparticles to obtain the binding probability for a given depletion layer thickness under defined flow condition.

Binding probability of nanoparticles as a function of depletion layer thickness is plotted in Fig. 2.8 for two different shear rates ($2s^{-1}$ and $10s^{-1}$). Fig. 2.8 (a) shows the simulation result of nanoparticle binding probability under a shear rate of $10s^{-1}$. The nanorod shows considerably higher binding probability than the nanosphere at both shear rates. As the depletion layer thickness increases, binding probability of nanoparticle decreases. Furthermore, due to limited diffusion length the binding probability of a nanosphere decreases almost linearly with depletion layer thickness, except for very low depletion layer thickness of 1.5 µm. At this thickness, the size of nanoparticle becomes comparable to the thickness size, thus transportation of nanosphere becomes diffusion dominant and resulting in high deposition probability. While the binding probability of nanorod decreases almost quadratically, mainly due to the tumbling motion. Furthermore, this result indicates that for a smaller depletion layer thickness, nanorod has significantly higher binding probability than nanosphere. As shear rate decreases, binding probability for both particles increases, since the diffusion motion becomes a dominating factor that enhances the binding events. Moreover, the less difference between binding probability of nanorod and nanosphere is observed at a shear rate of $2s^{-1}$, as shown in Fig. 2.8 (b). At lower shear rates Brownian motion becomes a governing factor, and thus contribution of tumbling motion becomes marginal compare to the diffusion motion.

*2.4.5. Influence of shear rate on binding probability for a given depletion layer thickness*

The binding probability of nanoparticles under different shear rate is studied for a given depletion layer thickness (5 µm). Binding probability as a function of shear rate for nanoparticles

with three different aspect ratios (1, 5 and 10) is plotted in Fig. 2.9. The simulation result elucidates that increase in shear rates reduces binding probability of nanoparticles, but the degree of reduction of binding probability varies with different nanoparticles. Results imply that binding probability rapidly drops for nanosphere with increase in shear rate. While that of nanorods drops only marginally with increase in shear rate. This result clearly demonstrates advantage of nanorod over nanosphere in terms of binding probability over a range of shear rates.

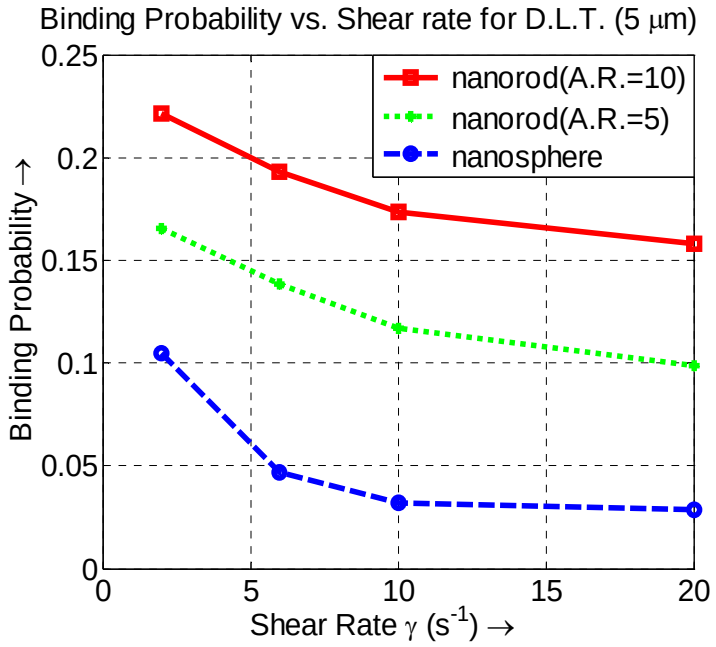


Figure 2.9 Studying effect of aspect ratio of nanoparticle on binding probability. Binding probability of nanorod and nanosphere under different shear rates for a depletion layer thickness of 5 μm is shown.

Fig. 2.9 also shows that nanorod with higher aspect ratio has higher binding probability than that with lower aspect ratio. Binding probability of nanorod with higher aspect ratio is boosted by much larger tumbling motion. To summarize, nanoparticle with high aspect ratio has higher binding probability and its binding probability decays slower with shear rate compared to that with low aspect ratio.

## 2.5 Nanoparticle deposition and distribution in an injured blood vessel

Another application of developed model is to determine nanoparticle deposition and distribution in real vascular geometry to validate *in vivo* efficiency of targeted drug delivery. To demonstrate capability of developed model in this work, a case similar to real targeted drug delivery at injured blood vessel site is developed and executed. When a portion of the blood vessel is injured, a significant P-selectin is expressed on damaged endothelial cells [96-99], which can be targeted by nanoparticles coated with GPIb ligand. Using that principle, targeted drug delivery is modeled with ~ 1000 particles in a blood vessel with an injured site as shown in Fig. 2.10 (a).

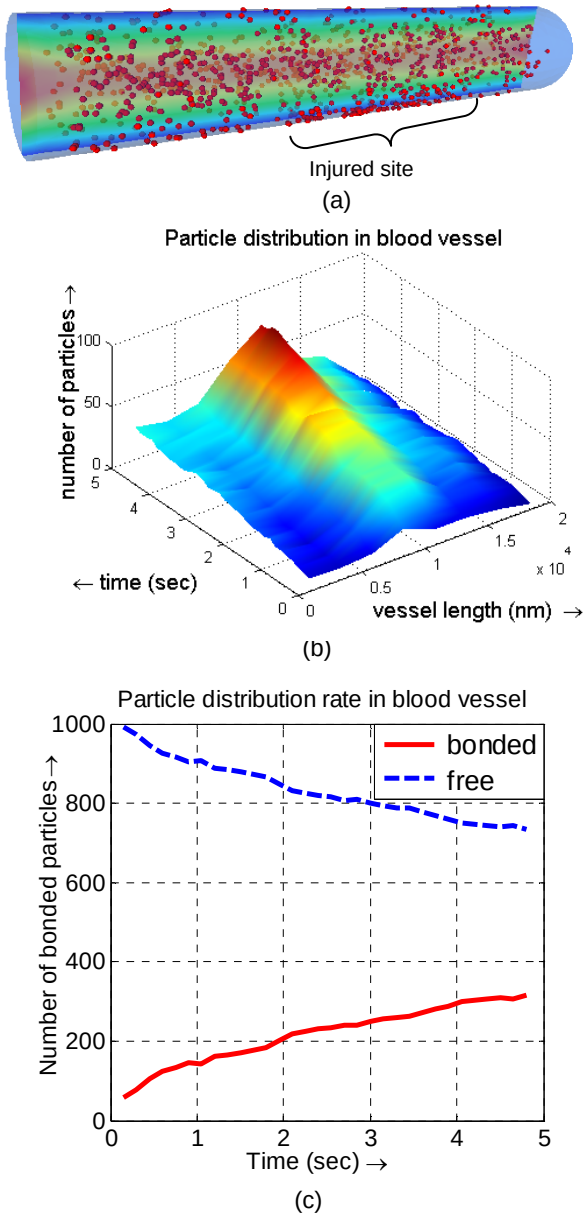


Figure 2.10 Multi-particle deposition and spatial distribution model. (a) Particle deposition distribution at an injured site; (b) 3D time history plot of particle distribution in blood vessel; (c) particle deposition as a function of time, average deposition rate is around 50.7 $s^{-1}$.

The convective transportation, Brownian motion, and deposition of multiple nanoparticles are clearly captured. The particle deposition distribution time history is plotted in Fig. 2.10 (b). The x-axis of the plot indicates the location of particle deposition over the blood

vessel length, y-axis shows the time of particle deposition at that location, and z-axis shows number of particle deposited at a given time and location. The number of particles deposited in the blood vessel is counted for a bin size of 2500 nm. The simulation result clearly shows a higher concentration of deposited nanoparticles at the injured region, with an average deposition rate of $50.7s^{-1}$, as shown in Fig. 2.10 (c). Both the distribution and deposition rate are a useful quantitative data that can be compared with designed experiments.

In this chapter, a numerical model named, nanoparticle brownian adhesion dynamics is developed. This model effectively describes the targeted drug delivery process. Using this developed numerical model the influence of nanoparticle shape, ligand density, and flow conditions on nanoparticle adhesion probability is explored. The results suggest that under similar flow conditions, the nanorods exhibit higher binding probability than that the nanospheres. Further elaboration of the results is discussed in Appendix. C.

# CHAPTER 3

## INTRODUCTION TO BIOSENSORS DETECTION METHOD

Biosensors are sensing devices to capture and detect biomolecules. Applications of biosensor include early detection of disease, glucose monitoring in diabetes patients, environmental application, etc. [100, 101]. In principle, Biosensors integrate electronic circuitry with natural molecules, such as antibodies, nucleic acid or DNA, as a sensing element which enable the devices to capture target molecules. Real-time biosensors can take multiple temporal measurements, thus allowing observation of the binding kinetics as well as a precise characterization of biomolecule concentration. In efforts to design more sensitive devices, researchers have created sensors with various geometries: planner, wire, sphere, etc, as shown in Fig. 3.1. Functional nanowire arrays constitute one of the most fascinating biosensor enabled by nanotechnology. The high surface to volume ratio associated with nanowires enhances the detection of the binding events between probe-antibodies and target molecules. In recent years, efforts have been made to develop a computation model of biosensor detection using continuum reaction-diffusion method [56, 102] to get insights of the Biosensing process. However, there are significant limitations associated with continuum model that will be discussed in following sections. The aim of this work is to explore theoretical mechanism of biosensor detection and to link it with experimental work for optimizing design of biosensors.

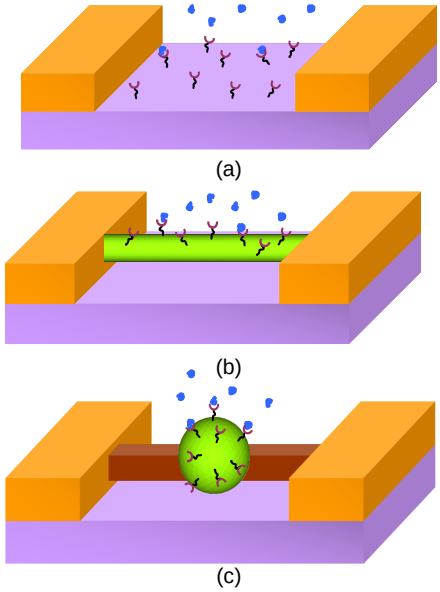


Figure 3.1 Different types of biosensors: (a) planar sensor (b) nanowire sensor (c) nanosphere sensor.

## 3.1 Continuum diffusion-reaction model

Most of the current detection methods for low concentration solutions are diffusion-limited. The time for detection is determined by the time required by the target molecules to reach and react with the probe molecules immobilized on the sensor surface, which is on the order of $\sqrt{Dt}$, with *D* the diffusion constant and *t* the settling or response time. Thus, the biochemical/affinity sensors are limited to a diffusion-limited process, which require a long-incubation time as the target molecules must travel to the arrayed probe on the sensor surface. Continuum convection-reaction-diffusion equation has been widely used to describe the biomolecule diffusion and binding process. The conservation equation for target analyte with concentration *c* and diffusivity *D* in a fluid flow with velocity *u* can be described as:

$$\frac{\partial c}{\partial t} = D\nabla^2 c - u \cdot \nabla c \qquad (2.20)$$

The binding process at the receptor coated surface can be described as:

$$\frac{\partial b}{\partial t} = k_{on} c_s (b_0 - b) - k_{off} b \qquad (2.21)$$

Where, $k_{on}$ is the binding constant, $k_{off}$ is the disassociation constant, $b$ is the surface concentration of bonded analyte, $c_s$ is the analyte concentration at the surface boundary, and $b_0$ is the density of probe molecules on the sensor. At relatively high analyte concentration (> nM) continuum theory agrees closely with experimental work, but accuracy of the continuum analysis vanishes at ultra low concentration. Using continuum models, a group of researchers [55, 56] claim that it may require a few days to detect a solution with concentration as low as 10 fM using nanowire sensor array. However, experiments have shown that even such low concentration can be detected within few minutes [45, 103]. This controversy between predictive results from continuum theory and actual experimental observation might be due to the possible breakdown of continuum theory at ultra low concentration. At ultralow concentration such as 1 fM, there could be only 1 target analyte present in a sample volume of about $10^6$ $\mu m^{-3}$ [58] (For the formulation refer to Appendix. B), which makes the continuum concentration treatment invalid. Though it might be argued that continuum theory gives the "average" solution of a large number of detection processes, yet, important features such as statistical variance and other possible contributing physical factors are not considered by the continuum. To explain the ultralow concentration detection dilemma from both statistical and physical point of views, a particulate Brownian binding model is used in this work.

### 3.2 Particulate brownian binding model for Biosensing

A particulate brownian binding model is used to describe the diffusion and binding process of target biomolecules on the biosensor surface. Brownian diffusion of small particles/target molecules is an inevitable phenomenon at the nanoscale, which causes target molecules to move freely within the solution. Once approaching the sensor surface, they bind with probe molecules on the sensor surface. Depending upon sensor's detection sensitivity, a detectable electrical signal is triggered upon a certain number of target molecules are bonded onto the sensor surface. Such detection signal are usually changes in resistance, impedance, or current [101, 104]. A large stochastic error is associated with biomolecules detection at ultralow

concentration. This is because the detection signal is triggered by just a few random binding events [55, 57]. To capture such rare events, it is more reasonable to track motion and binding of individual target molecules by using a particulate method instead of using a continuum concentration description. Moreover, it is easier to explore through a particulate method the possible contribution of other physical mechanisms such as electrical forces or fluid flow.

*3.2.1. Molecule binding kinetics*

A kinetic reaction model is used to describe the binding process. The binding process between target molecule and receptor on the surface is governed by monovalent kinetic forward ($k_{on}$) and reverse ($k_{off}$) reaction rates.

$$k_{on} = k_f^0 \exp\left(-k_{ts} L^2 / 2B_z\right) \tag{2.22}$$

$$k_{off} = k_r^0 \exp\left(-(\sigma - k_{ts}) L^2 / 2B_z\right) \tag{2.23}$$

Where, $\sigma$ is the bond elastic constant; $k_{ts}$ is the bond elastic constant at transient state; $B_z$ is thermal energy; $k_r^0$ and $k_f^0$ are the reverse and forward reaction rates at zero load of target molecule-receptor pair, respectively; $L$ is the difference of bond length y and equilibrium length λ. These constants values are mentioned in Table.1 of chapter 2. In this model, bonds form and break according to empirical statistical laws [105]:

$$P_f = 1 - \exp(k_{on}.\Delta t) \tag{2.24}$$

$$P_r = 1 - \exp(k_{off}.\Delta t) \tag{2.25}$$

Where, $P_f$ is the forward (bond formation) probability and $P_r$ is the bond breaking probability. For each time step, bond formation and breakage are simulated using a Monte Carlo process, in which bond formation and breakage occur if random numbers are chosen that are less than the probabilities $P_f$ and $P_r$ for binding and unbinding, respectively, in the time interval [106].

*3.2.2. Brownian dynamics under fluid flow*

A particle suspended in a fluid experiences a hydrodynamic force due to the average motion of the fluid around it. The average motion of the fluid is represented by the continuum Navier– Stokes equations. Small particles in fluids, in addition to the average force, experience a random force due to the thermal fluctuations in the fluid. In Brownian dynamic (BD) simulations, the thermal force from the fluid is described by the second fluctuation dissipation theorem [107] and integrated along with molecule binding kinetics in the IFEM platform [64, 65]. With its stochastic nature, Brownian dynamics model can mimic the real detection process, which is dominated by random initial position of the molecules as well as the random diffusion/binding process. The random force expression and the particle motion dynamics are treated same as described in chapter. 2.

## 3.3 Simulation results of Biosensor numerical model

The following simulation studies are performed on planar and/or nanowire sensor. The set up comprised of three components: (1) fluid domain (2) sensor surface, and (3) randomly distributed target molecules (effectively represented as a sphere of 50 nm diameter), as shown in Fig. 3.2. The number of particles will be determined by the target concentration under consideration. The formula to covert the target concentration in to a number of particles is mentioned in Appendix. C. The dimension and mesh information of the fluid domain can be found in Appendix (A.3 & A.4).

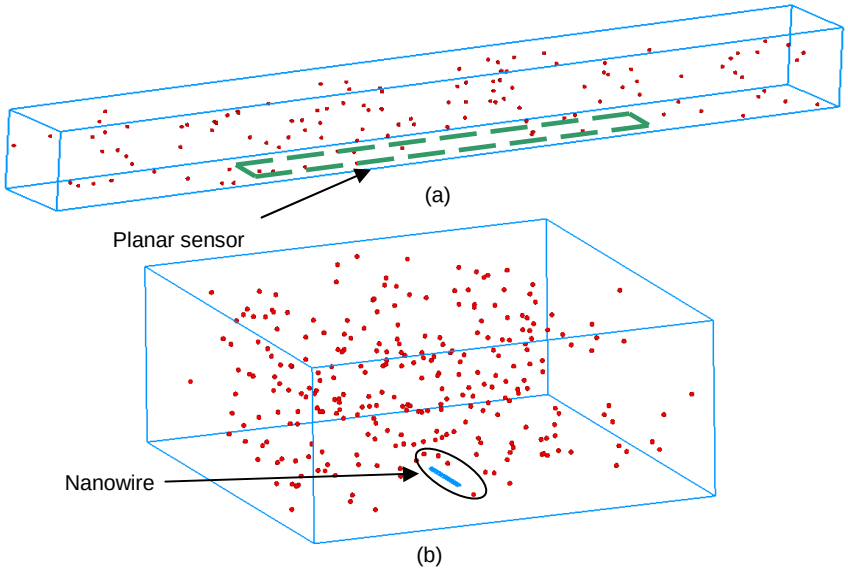


Figure 3.2 Model set up for biosensors (a) Shows domain and planar sensor (10 µm x 1 µm) (b) Shows domain and nanowire sensor at bottom (10 µm x 50 nm)

*3.3.1. Effect of target molecules interaction on deposition rate*

Effect of particle interactions on deposition rate is studied first to check if interactions between freely moving and bonded particles influence particle distribution and deposition. For simplicity, the inter-particle interaction is modeled as a repulsive Lennard-Jones (LJ) potential. Simulation result with and without inter-particle interactions is plotted in Fig. 3.3. The effect of inter-particle interaction on particle deposition over time is shown to be negligible. Thus, inter-particle interaction is not included in this study for the rest of this chapter.

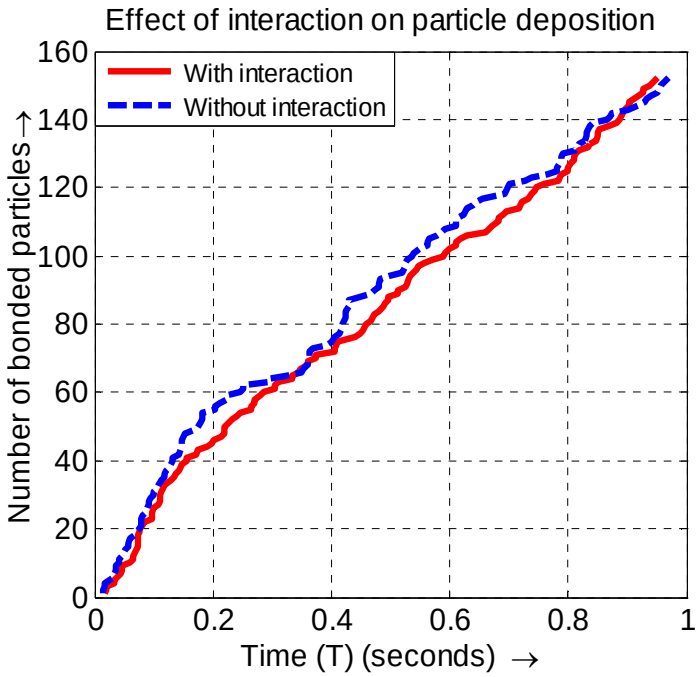


Figure 3.3 Particles deposition as a function of time at 15 nM concentration for two different cases; one is with interaction and one without interaction. Interaction between freely moving particle and bonded particles is considered.

*3.3.2. Statistical variance in detection time at low concentration*

At ultralow concentration, the detection process is composed of a sequence of random binding events. In this section, the statistical variance associated with detection at low concentration is investigated, which is an important feature of the detection process, yet neglected and unable to be captured by the continuum diffusion theory. The binding time histories of 10 independent trials at 2.5nM concentration are plotted in Fig. 3.4 (a). Each trial starts with ~ 120 molecules randomly distributed in a 20 µm by 2 µm by 2µm rectangular block domain.

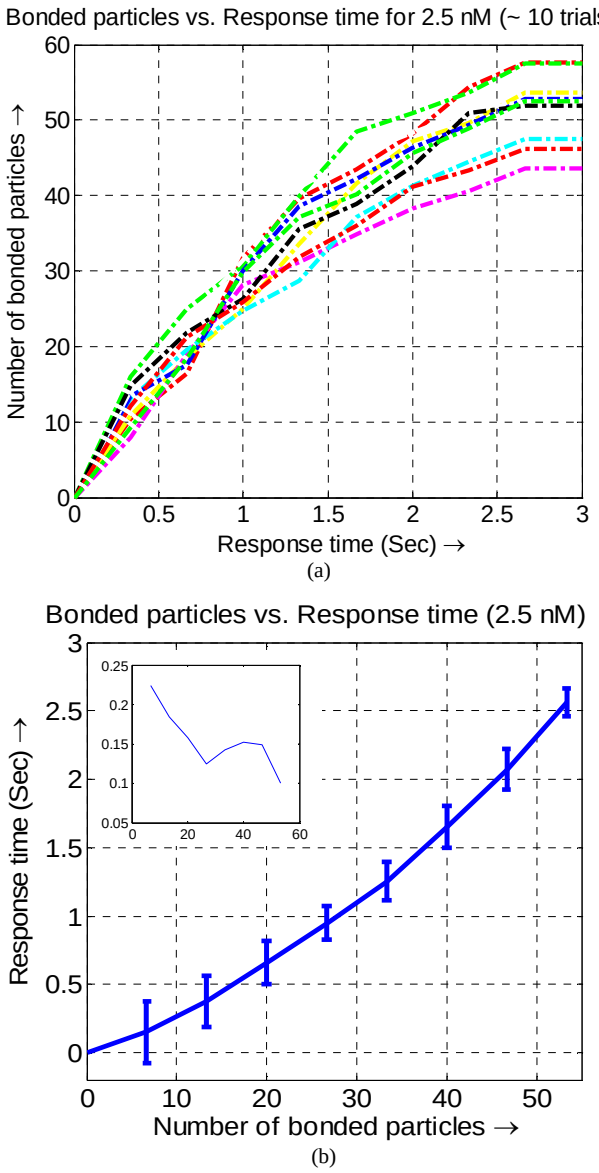


Figure 3.4 The response time required for deposition of a certain number of particles to trigger detectable signal at 2.5nM concentration. (a) Time history plot of 10 independent deposition trials (b) Response time as a function of number of bonded particles required to trigger detectable signal for 10 independent trials. The mean and standard derivation of the response time is shown. The standard deviation is normalized by divided with the mean value.

The result clearly shows that the binding process is a stochastic process. Under a given concentration, the detection time for a given number of bonded particles fluctuates. In correspondence, the mean response time required for accumulate a certain number of bonded

particles are plotted in Fig. 3.4 (b). The variation in response time decreases with the number of particles required for triggering detection signal. This indicates that the more sensitive the sensor is, the larger the response time variance. This is because while the binding of individual particles is random, the collective binding result of a large number of particles is determinant.

*3.3.3. Effect of sensor design on detection response time*

In this study, performance of a planar and a nanowire sensor is compared for a given target analyte concentration. The set information is mentioned in Fig. 3.2. The response time as a function target analytes concentration simulated by brownian binding model is plotted in Fig. 3.5 (squares and circular marks). The solution from continuum diffusion-reaction model is also plotted in Fig. 3.5 (red and blue lines for planar and nanowire cases, respectively).

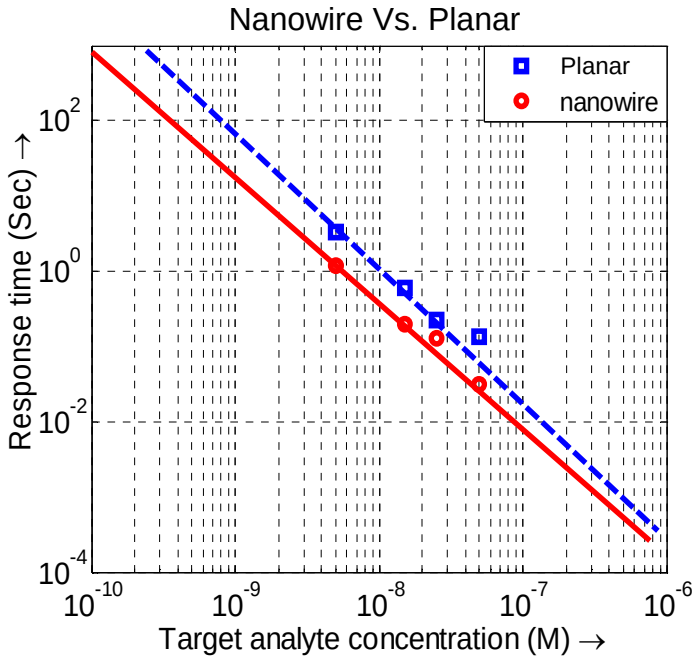


Figure 3.5 Comparison of detection time of nanowire and planar sensor.

For the given concentration, the response time of nanowire is lower than that of planar sensor that suggests nanowire sensor has higher sensitivity than the planar sensor. Moreover, the response time decreases linearly with the molecular concentration, which agrees with the

Alam's work [58]. Finally, this simulation results demonstrates the developed particle model agrees with continuum model at high analytes concentrations.

### 3.4 Electroosmosis assisted Biosensing

Biosensing application is always under an applied electric field. Surfaces of the microchannel in contact with an aqueous solution usually have electrostatic charges. The surface charge in turn attracts the counter-ions in the liquid to the region close to the surface, forming a electric double layer (EDL) [108, 109]. The electrostatic force applied to the charged double layer on the surfaces of the electrodes generates electroosmotic flow. In this preliminary study, the electroosmotic flow is treated as a slip boundary condition for the fluid. Also, since the Debye layer (the layer close to the wall where the velocity is varying) is only a few nanometers, only the steady velocity is taken into account:

$$\mathbf{v} = -\varepsilon_f \psi_0 \mathbf{E} \big/ \mu \qquad (2.26)$$

Where, $\psi_0$ is the zeta potential, $\mu$ is the fluid viscosity, and $\varepsilon_f$ is the fluid permittivity. When a DC or low frequency AC field is applied on a pair of parallel rectangular-shaped electrodes with a 10μm gap, local electroosmotic flow near the edges of electrodes is found to induce vortices. It is expected that such electroosmosis flow induced vortex will help transport all nearby molecules toward the electrode edge, which may significantly reduce detection time at ultralow concentrations where the target molecules are very few in numbers and might be far away from the sensor surface.

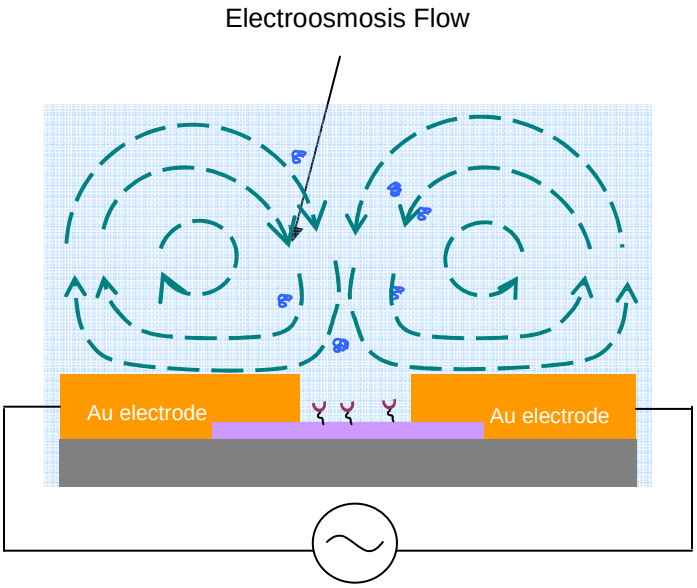


Figure 3.6 The set up of electroosmosis assisted biosensor. Electroosmosis flow is generated on surfaces of the two bottom electrodes.

To validate this hypothesis, a quantitative study is made on electroosmosis flow assisted biosensors and to compare it with poiseuille flow assisted biosensors. In the following study, biosensor placed at the bottom of a rectangular block filled with a solution of ~ 1.5 pM is considered, as shown in Fig. 3.6. To ensure statistical accuracy, the sensor response time is evaluated based on 10 independent trials.

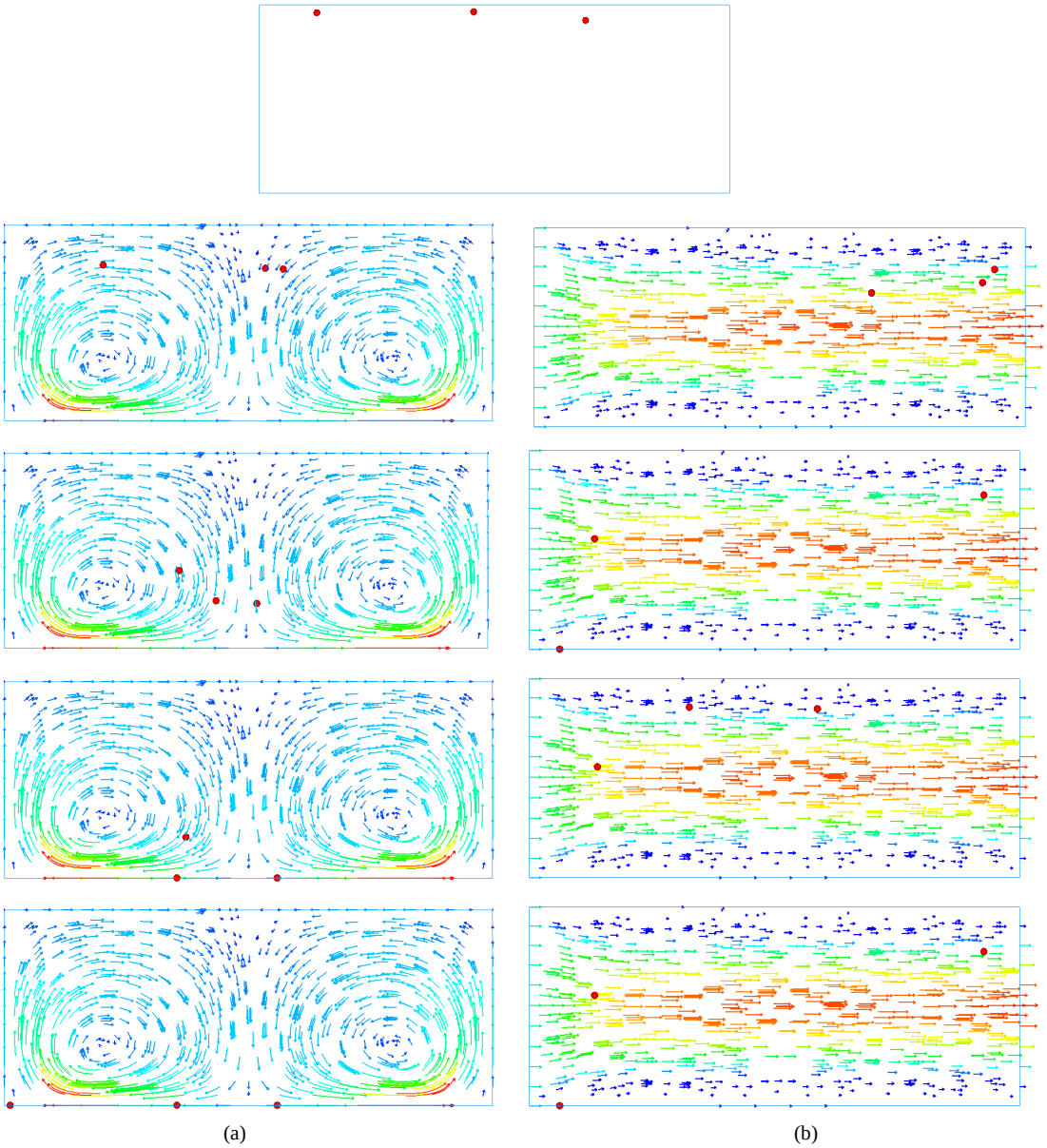


Figure 3.7 Detection of 1.5pM solution under electroosmosis flow and poiseuille flow. (a) Flow field and particle motion of electroosmosis flow assisted biosensor; (b) Flow field and particle motion under a poiseuille flow of 5 um/s at t=1s, 5s, 10s and t=15s, respectively.

For both electroosmosis flow assisted and poiseuille flow assisted sensors, the same initial configuration is considered, as shown in Fig. 3.7. Three molecules are randomly positioned on top of the domain. The detection process of both sensors is qualitatively

compared. The difference of detection method is evident from the instantaneous snapshots taken at 4 different time intervals.

To trigger the detection signal, target molecules bonded to the sensor surface need to exceed a certain number depending upon sensor property. The sensor response time as a function of triggering bonded target molecules under 1.5pM concentration is plotted in Fig. 3.8.

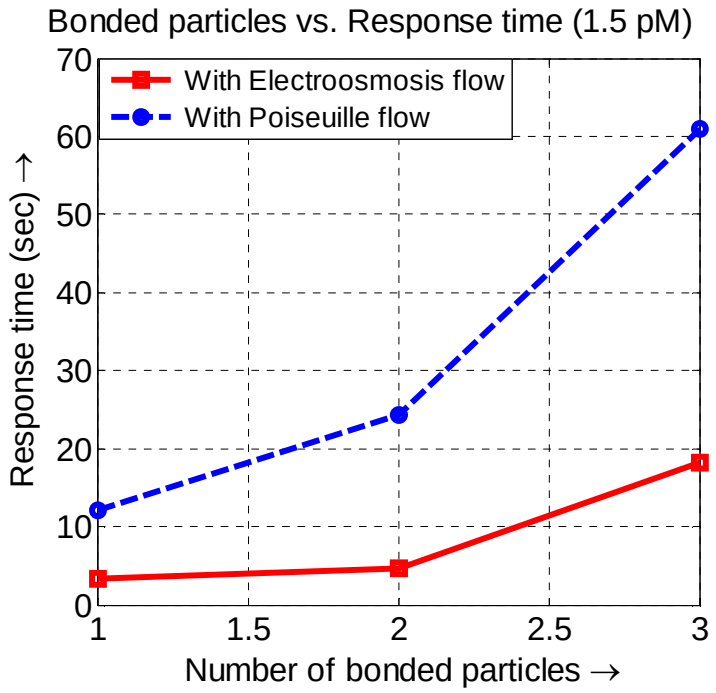


Figure 3.8 The response time of two different types of biosensors for 1.5 pM concentration; solid line plot is for electroosmosis flow assisted biosensor and dashed line plot is for poiseuille flow assisted biosensor.

The detection time of electroosmosis flow assisted biosensor is less than half of that required by poiseuille flow assisted biosensor. For ultra low concentration, there might be just one target molecule in the solution domain. Thus, target molecules have to travel a long distance to reach near to the sensor surface. So, in case of poiseuille flow assisted biosensor transportation of analyte becomes diffusion limited. While, in case of electroosmosis flow, vortex flow actually bring over target molecules from far field to be near to the sensor surface in much shorter time. The difference in response time is expected to be even larger at fM concentration.

# CHAPTER 4

# CONCLUSION AND FUTURE WORK

## 4.1 Nanoparticle brownian adhesion dynamics

Mathematical modeling of targeted drug delivery system provides quantitative descriptions of the drug transportation in biological systems. It can be utilized to evaluate efficiency of drug delivery, and to estimate dose response and toxicity. To capture underlying transportation and deposition mechanism, a novel multi-scale computational modeling tool has been developed. The adhesion kinetics of nanoparticle coupled with Brownian Dynamics is studied for the first time with a three-dimensional hydrodynamic simulation method. While the focus here has been on the rod-shaped nanoparticles, this method is applicable to any arbitrarily shaped nanoparticles.

The numerical model based on the probabilistic kinetic formulation has been developed. Adhesion probability of four different shaped particles, rod, disk, oblate, and spherical, has been compared. The result elucidates that non-spherical shape particles has remarkably higher adhesion probability compare to its counterpart spherical for a given particle volume. The disc shaped nanoparticles have shown highest drug loading capability among all other nanoparticles. Even the rod shaped nanoparticle demonstrated considerably high adhesion probability compare to the spherical particle. Thus, theoretical result indicates the nanoparticle shape plays a vital role in targeted drug delivery efficiency. From the theoretical expression of adhesion probability, the dissociation probability of nanoparticle is determined. The dissociation probability of the nanosphere is found to be larger than that of nanorod for a given shear rate. In summary, the theoretical predictions indicate that nanorod exhibit higher adhesion probability compare to its spherical counterpart. Thus, nanorod is an appropriate choice for the targeted drug delivery application.

The influence of nanoparticles shape and ligand density on nanoparticle adhesion kinetics has been studied qualitatively. The simulation result demonstrates the ability of non-spherical nanoparticle to adhere to the vascular wall surface due to tumbling motion whereas spherical particle just flows away without interacting to the wall surface. Furthermore, upon initial contact the stability of nanoparticle, whether it remains adhere or not, is dictated by the ligand density. The result reveals that nanoparticle with low ligand density gets unbounded due to weak adhesive force, but nanoparticle with high ligand density firmly adheres to the wall surface under the same physical condition. The statistical variance of nanoparticles trajectory shows that non-spherical particles have higher fluctuation in their trajectories compare to their spherical counter parts. Thus, non-spherical particle will have more number of binding events compare to spherical particle during its transportation through the channel.

Binding probability of nanorods and nanospheres is determined for a range of depletion layer thickness. It is found that nanorod has considerably higher binding probability compare to nanosphere under the same flow condition. Moreover, with increase in shear rate the difference of adhesion probability between nanorod and nanosphere is found to be increasing.

To sum up, nanorods are found to have a higher chance of contact with wall surface then that of nanosphere under similar vascular flow condition, mainly due to the tumbling motion. Such knowledge can be used to optimize the design of shape and size of nanoparticle for desired nanomedicine functions. Finally, in depth analysis using developed may help to shorten the cycle for the design of nanomedicine carriers for a variety of useful applications.

## 4.2 Future work: Evaluation of Targeted drug delivery efficiency

An advanced model will be developed to include blood cells into the analysis, thus, the influence of cell-particle interaction would be studied for the first time. This model will determine the coefficient called as dispersion coefficient, a parameter governing particles concentration near to wall region. Once that is achieved, it would be combined with the deposition rate at near wall region to get predict targeted drug delivery efficiency. In addition, the focus would be to

design nanoparticles for targeted delivery to affected sites and predict its distribution under idealized vascular environment. To mimic the real geometry, the vascular environment will be reconstructed from original CT/MRI images. In support of this idea, a preliminary result of nanoparticle deposition in a two-branch vessel is shown in Fig. 4.1. A non-uniform nanoparticle deposition distribution is observed on vascular surface, with a high particle concentration on the bifurcation region. The multiscale fluid mechanics and binding kinetic models will be developed to address the coupling between the physics at these two scales. Model predictions will be validated against experimental and clinical data from designed experiments. Thus, the ultimate goal of this study would be for given patient vascular network, to design nanoparticles for maximum targeting efficiency and minimum drug dosage to reduce any risk of damaging surrounding cells and reduce overall health care cost.

Figure 4.1 Particle deposition and distribution in real vascular geometry

## 4.3. Physics of Biosensor Detection

Biosensors are micro/nano scale devices employing biochemical molecular recognition properties as their basis for a selective analysis. Researchers have been investigating the potential of nanoscale biosensors for label-free and ultra sensitive detection of target biomolecules. However, to achieve this goal through experimental study is very challenging; thus, exploring the detection process via a computational approach is more convenient. The role of continuum reaction-diffusion model at ultra low concentration detection is questionable. Thus, particulate brownian binding model is developed to predict the performance of biosensors, in particular for ultra low concentration. Computational modeling tool model describes the transportation and binding process of the target molecule on the biosensor surface. The motion of target molecules is governed by fluid flow and brownian dynamics, whereas the binding process is described by molecular adhesion kinetics.The effect of interactions between freely moving and bonded particles on particle distribution is studied. The result indicated that the effect of inter-particle interaction on distribution and deposition rate is negligible. This simplifies future simulation by neglecting inter-particle interaction. Further, the binding histories of 10 independent trials have been compared and for a given response time significant variation in number of bonded particles is observed. It implies that the detection process at low concentration is a stochastic process. Moreover, the statistical variance of the detection process of an individual target molecule is captured, which is not possible to determine using continuum theory. Performance of a nanowire and a planar nanosensor is compared. The results shown that nanowire sensor has lower response time than planar sensor for a given concentration. Thus, it indicates that nanowire sensor could be a better choice for detection at ultra low concentration.

The dilemma of detection limit could be explained by the electroosmosis flow. In a preliminary study, response time of electroosmosis assisted and poiseuille assisted biosensor is compared. The result elucidates that electroosmosis flow enhances the biosensor performance.

The electroosmosis flow assisted biosensor found to be almost 3 times sensitive than the poiseuille assisted biosensors at 1.5pM. At fM concentration, it is expected that electroosmosis flow assisted biosensor may have very low detection time and eventually theoretical prediction may agree with the experimental results at the end.

### 4.4. Future work: Reducing response time for biosensor detection

Future work would be focused on developing model that utilizes electroosmosis flow principle to simulate biosensor detection. Theoretical predictions will be compared with experimental results, to ensure consistency among the results. That could help for the better design of biosensors.

Further, electric field assisted biosensor, such as dielectrophoresis assisted sensor, will be developed. Researchers have demonstrated manipulation of biomolecules or microparticles using dielectrophoresis and shown that it can increase sensitivity of respective biosensor [110-112]. Depending upon biomolecules electrical property, dielectrophoresis can provide controlled manipulation of those biomolecules to enhance biosensor performance. A numerical model will be developed to investigate the effect of dielectrophoresis, and its impact on the sensitivity of the sensor will be studied.

The fully established computational model of the biosensor will provide enormous opportunity of studying different types of biosensor theoretically and characterize its performance without bothering to study it experimentally.

# APPENDIX A

## MESH INFORMATION

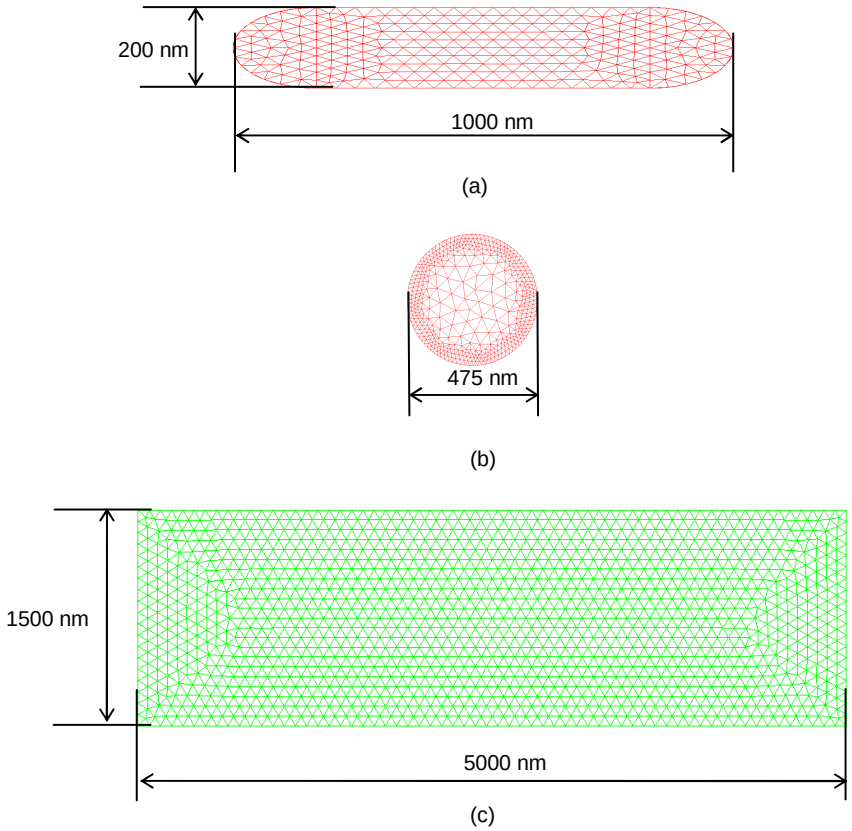


A.1: Meshes and dimensions of nanoparticles and fluid domain (a) Nanorod (node: 1404 and elements: 5996), (b) Spherical nanoparticle (node: 3213 and elements: 14286), (c) fluid channel (node: 1017 and elements: 2870)

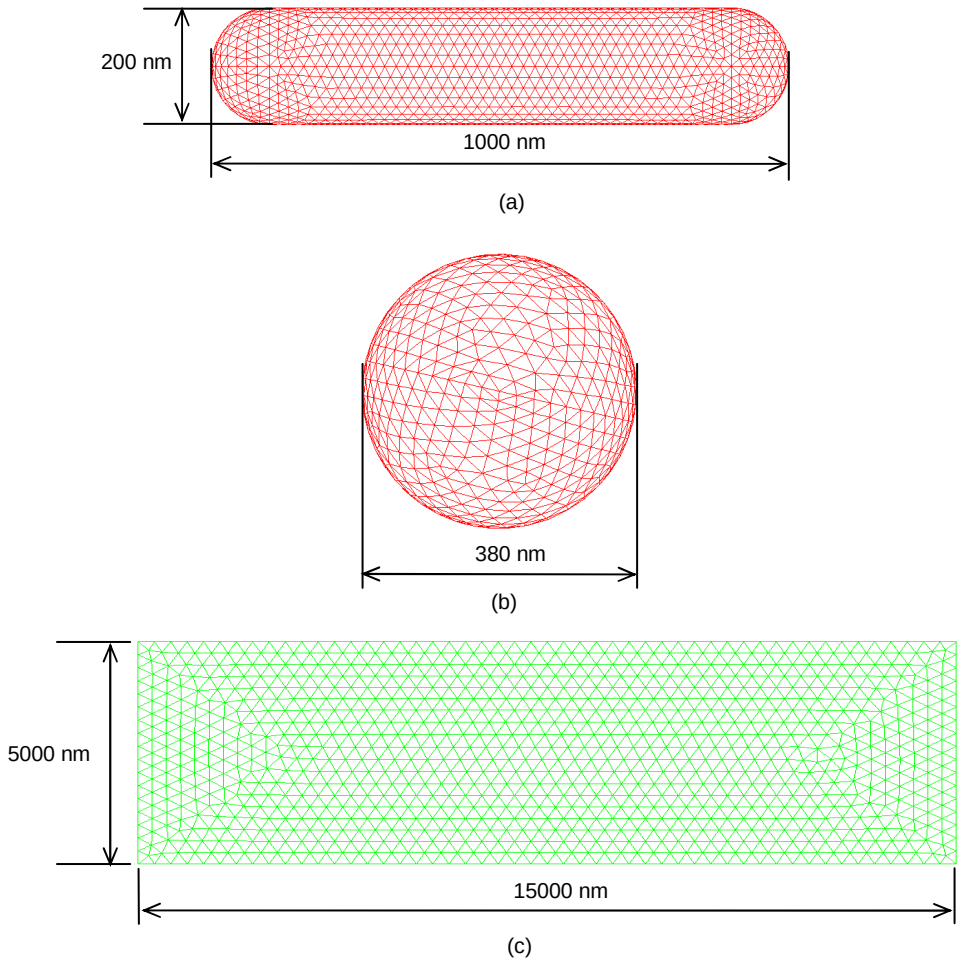


A.2: Meshes and dimensions of nanoparticle and fluid domain (a) Nanorod (node: 4680 and elements: 22457), (b) Nanosphere (node: 2194 and elements: 10818), (c) fluid channel (node: 2044 and elements: 5739)

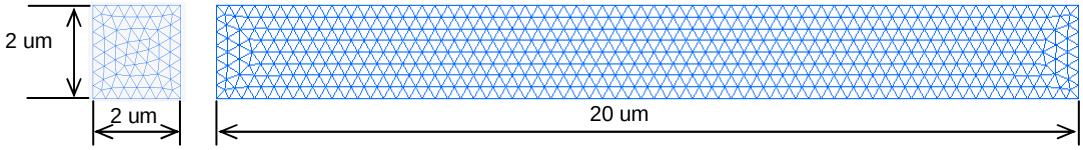


A.3: Mesh and dimension of planar sensor (node: 5444 and elements: 25801)

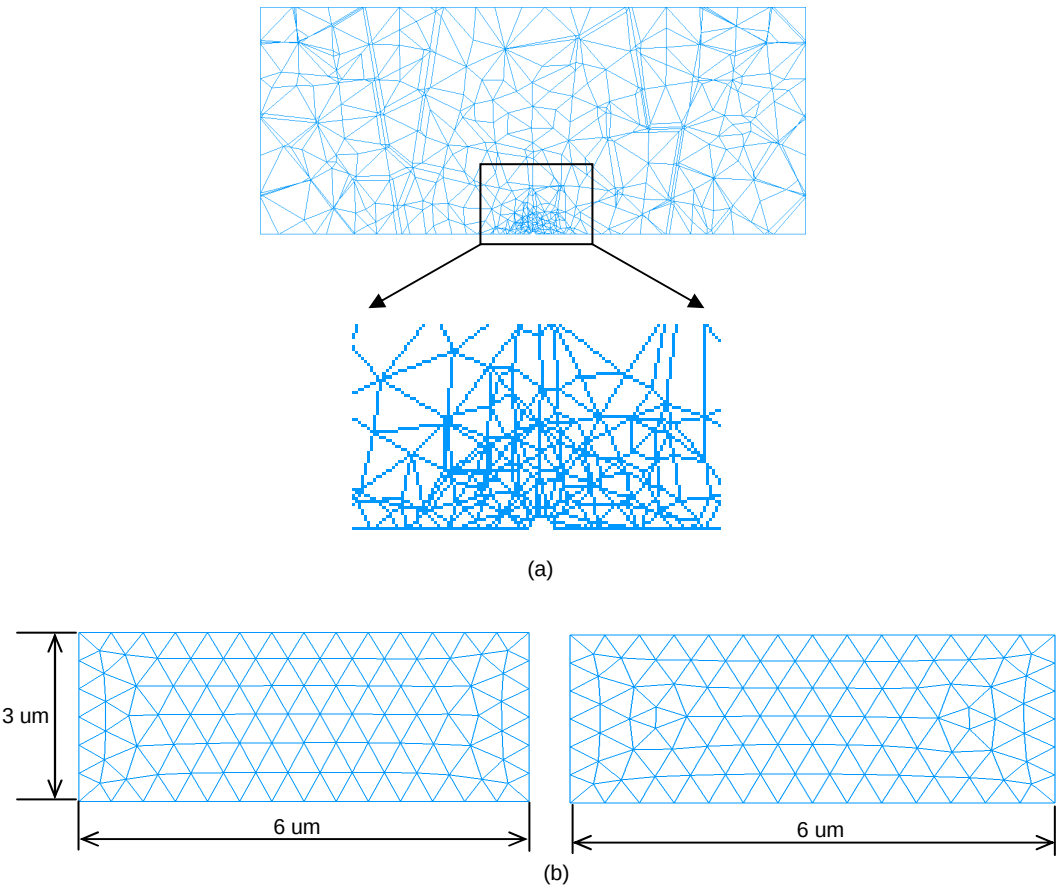


A.4: Nanowire sensor (node: 3103 and elements: 15019) (a) Cross-sectional view of the fluid domain with expended view of nanowire cross-section, (b) Mesh and dimension of the fluid domain

# APPENDIX B

## CALCULATION OF NORMALIZED BINDING RATE

Physically, the binding rate means the number of particles deposited in one second, and it is mainly governed by the chemical reaction. But, it is unable to capture the dynamic convection-diffusion process. Therefore, another parameter named normalized binding rate is developed and determined from the simulation results. This parameter effectively includes the convection-diffusion process. First, the average time of a single trial is calculated from the channel length and the velocity. Then, the following equation is used to calculate the normalized binding rate (NBR):

$$NBR = \frac{total\ number\ of\ deposited\ particles}{Total\ number\ of\ particle\ gtime_{avg}}$$

The results have been summarized in following table:

| Binding rate | | | | |
|---|---|---|---|---|
| | Nanosphere | | Nanorod | |
| Thickness (μm) | For $2s^{-1}$ | For $10s^{-1}$ | For $2s^{-1}$ | For $10s^{-1}$ |
| 1.5 | 0.1078 | 0.2512 | 0.1714 | 0.5566 |
| 2.5 | 0.0794 | 0.1632 | 0.1020 | 0.4228 |
| 4.0 | 0.0796 | 0.1504 | 0.1072 | 0.3810 |
| 5.0 | 0.0700 | 0.1070 | 0.1101 | 0.3894 |
| 6.0 | 0.0574 | 0.1000 | 0.1115 | 0.3951 |

The significance of the NBR is that it suggests how fast the particles will bind to the surface. It can be interpreted as out of total particles present within defined depletion layer thickness, the number of particles deposited in one second for a given shear rate. Further, average time considered in the calculation might be longer than the actual one, because particle may get bind before the average time. Thus, the value of the calculated NBR is underestimated.

# APPENDIX C

## CONCENTRATION CONVERSION FORMULA

Following is the formula to convert given concentration into number of particles.

$$N = \frac{N_A \cdot Vol \cdot C_o}{10^{-3}}$$

Where, *N* is the total number of target molecules, *vol* is the volume of fluid domain under consideration, *Na* is Avogadro's number (6.022 x $10^{23}$ $mol^{-1}$), and $C_o$ is target analytes concentration in Molar.

REFERENCES


1. Chauvierre, C., et al., Novel polysaccharide-decorated poly(isobutyl cyanoacrylate) nanoparticles. Pharmaceutical Research, 2003. 20(11): p. 1786-1793.
2. Farokhzad, O.C. and R. Langer, Nanomedicine: Developing smarter therapeutic and diagnostic modalities. Advanced Drug Delivery Reviews, 2006. 58(14): p. 1456-1459.
3. Mathiowitz, E., et al., Biologically erodable microsphere as potential oral drug delivery system. Nature, 1997. 386(6623): p. 410-414.
4. Nasongkla, N., et al., Multifunctional polymeric micelles as cancer-targeted, MRI-ultrasensitive drug delivery systems. Nano Letters, 2006. 6(11): p. 2427-2430.
5. Roney, C., et al., Targeted nanoparticles for drug delivery through the blood-brain barrier for Alzheimer's disease. Journal of Controlled Release, 2005. 108(2-3): p. 193-214.
6. Shah, P., Use of nanotechnologies for drug delivery. Mrs Bulletin, 2006. 31(11): p. 894-899.
7. Sukhorukov, G.B. and H. Mohwald, Multifunctional cargo systems for biotechnology. Trends in Biotechnology, 2007. 25(3): p. 93-98.
8. Liu, Y., W.L. Lu, and Q. Zhang, [Recent advances in liposomes and nanoparticles as drug carriers for drug delivery]. Zhongguo Yi Xue Ke Xue Yuan Xue Bao, 2006. 28(4): p. 583-9.
9. Sharma, G., et al., Liposomes as targeted drug delivery systems in the treatment of breast cancer. J Drug Target, 2006. 14(5): p. 301-10.
10. Maysinger, D., et al., Fate of micelles and quantum dots in cells. Eur J Pharm Biopharm, 2007. 65(3): p. 270-81.
11. Sutton, D., et al., Functionalized micellar systems for cancer targeted drug delivery. Pharm Res, 2007. 24(6): p. 1029-46.
12. Torchilin, V.P., Targeted polymeric micelles for delivery of poorly soluble drugs. Cell Mol Life Sci, 2004. 61(19-20): p. 2549-59.
13. Gao, X., et al., In vivo molecular and cellular imaging with quantum dots. Curr Opin Biotechnol, 2005. 16(1): p. 63-72.
14. Smith, A.M., et al., Engineering luminescent quantum dots for in vivo molecular and cellular imaging. Ann Biomed Eng, 2006. 34(1): p. 3-14.
15. Koenig, S. and V. Chechik, Shell cross-linked Au nanoparticles. Langmuir, 2006. 22(11): p. 5168-73.
16. Lou, X., C. Wang, and L. He, Core-shell Au nanoparticle formation with DNA-polymer hybrid coatings using aqueous ATRP. Biomacromolecules, 2007. 8(5): p. 1385-90.
17. Yang, Y., et al., Template guided self-assembling two-dimensional array of Au@SiO2 core-shell nanoparticles for room-temperature single electron transistors. J Nanosci Nanotechnol, 2005. 5(2): p. 179-83.

18. Cheng, Y., et al., Dendrimer-based prodrugs: design, synthesis, screening and biological evaluation. Comb Chem High Throughput Screen, 2007. 10(5): p. 336-49.
19. Duncan, R. and L. Izzo, Dendrimer biocompatibility and toxicity. Adv Drug Deliv Rev, 2005. 57(15): p. 2215-37.
20. Najlah, M. and A. D'Emanuele, Crossing cellular barriers using dendrimer nanotechnologies. Curr Opin Pharmacol, 2006. 6(5): p. 522-7.
21. Barge, A., et al., Rod-like shape of vesicular stomatitis virus matrix protein. Virology, 1996. 219(2): p. 465-70.
22. Gamliel, H. and A. Polliack, Virus-cell interactions as seen by scanning electron microscopy. Isr J Med Sci, 1979. 15(8): p. 647-52.
23. Jin, H., et al., Influenza virus hemagglutinin and neuraminidase cytoplasmic tails control particle shape. EMBO J, 1997. 16(6): p. 1236-47.
24. Kam, Z. and I. Gafni, Three-dimensional reconstruction of the shape of human wart virus using spatial correlations. Ultramicroscopy, 1985. 17(3): p. 251-62.
25. Ruigrok, R.W., et al., Natural heterogeneity of shape, infectivity and protein composition in an influenza A (H3N2) virus preparation. Virus Res, 1985. 3(1): p. 69-76.
26. Schneemann, A., The structural and functional role of RNA in icosahedral virus assembly. Annu Rev Microbiol, 2006. 60: p. 51-67.
27. Geng, Y., et al., Shape effects of filaments versus spherical particles in flow and drug delivery. Nature Nanotechnology, 2007. 2(4): p. 249-255.
28. Champion, J.A. and S. Mitragotri, Role of target geometry in phagocytosis. Proc Natl Acad Sci U S A, 2006. 103(13): p. 4930-4.
29. Calvo, P., et al., Long-circulating PEGylated polycyanoacrylate nanoparticles as new drug carrier for brain delivery. Pharmaceutical Research, 2001. 18(8): p. 1157-1166.
30. Kukowska-Latallo, J.F., et al., Nanoparticle targeting of anticancer drug improves therapeutic response in animal model of human epithelial cancer. Cancer Research, 2005. 65(12): p. 5317-5324.
31. Heidel, J.D., et al., Administration in non-human primates of escalating intravenous doses of targeted nanoparticles containing ribonucleotide reductase subunit M2 siRNA. Proceedings of the National Academy of Sciences of the United States of America, 2007. 104(14): p. 5715-5721.
32. E.F. Grabowski, L.I.F.a.E.F.L., Effects of shear rate on the diffusion and adhesion of blood platelets to a foreign surface. Ind. Eng. Chem. Fundam., 1972. 11: p. 224-231.
33. Vincent T. Turitto, A.M.B., Edward F. Leonard, Platelet Diffusion in Flowing Blood. Ind. Eng. Chem. Fundamen., 1972. 11(2): p. 216-223.
34. Tilles, A.W. and E.C. Eckstein, The near-Wall Excess of Platelet-Sized Particles in Blood-Flow - Its Dependence on Hematocrit and Wall Shear Rate. Microvascular Research, 1987. 33(2): p. 211-223.
35. Zhang, J.F., P.C. Johnson, and A.S. Popel, Effects of erythrocyte deformability and aggregation on the cell free layer and apparent viscosity of microscopic blood flows. Microvascular Research, 2009. 77(3): p. 265-272.

36. Aris, R., On the dispersion of a solute in a fluid flowing through a tube. Proceedings of the Royal Society of London Series A-Mathematical and Physical Sciences, 1956. 235(1200): p. 67-77.
37. Taylor, G., Dispersion of Soluble Matter in Solvent Flowing Slowly through a Tube. Proceedings of the Royal Society of London, Series A-Mathematical and Physical Science, 1953. 219(1137): p. 186-203.
38. Dembo, M., et al., The Reaction-Limited Kinetics of Membrane-to-Surface Adhesion and Detachment. Proceedings of the Royal Society of London Series B-Biological Sciences, 1988. 234(1274): p. 55-83.
39. Dong, C., et al., Mechanics of leukocyte deformation and adhesion to endothelium in shear flow. Annals of Biomedical Engineering, 1999. 27(3): p. 298-312.
40. Haun, J.B. and D.A. Hammer, Quantifying nanoparticle adhesion mediated by specific molecular interactions. Langmuir, 2008. 24(16): p. 8821-8832.
41. S. Shah, Y.L., W. Hu, J. Gao, Adhesion Dynamics of Functional Nanoparticles for Targeted Drug Delivery, in 25th Southern Biomedical Engineering Conference 200, A.L. McGoron, Chenzhong; Lin, Wei-Chiang Editor. 2009, Springer: Miami, FL. p. 386.
42. The Chipping forecast. Nature Genetics, 1999. 21(1).
43. The Chipping forecast II. Nature Genetics, 2002. 32(4).
44. Squires, T.M. and S.R. Quake, Microfluidics: Fluid physics at the nanoliter scale. Reviews of Modern Physics, 2005. 77(3): p. 977-1026.
45. Hahm, J. and C.M. Lieber, Direct ultrasensitive electrical detection of DNA and DNA sequence variations using nanowire nanosensors. Nano Letters, 2004. 4(1): p. 51-54.
46. Li, Z., et al., Sequence-specific label-free DNA sensors based on silicon nanowires. Nano Letters, 2004. 4(2): p. 245-247.
47. Li, Z., et al., Silicon nanowires for sequence-specific DNA sensing: device fabrication and simulation. Applied Physics a-Materials Science & Processing, 2005. 80(6): p. 1257-1263.
48. Cui, Y., et al., Nanowire nanosensors for highly sensitive and selective detection of biological and chemical species. Science, 2001. 293(5533): p. 1289-1292.
49. Zheng, G.F., et al., Multiplexed electrical detection of cancer markers with nanowire sensor arrays. Nature Biotechnology, 2005. 23(10): p. 1294-1301.
50. Bunimovich, Y.L., et al., Quantitative real-time measurements of DNA hybridization with alkylated nonoxidized silicon nanowires in electrolyte solution. Journal of the American Chemical Society, 2006. 128(50): p. 16323-16331.
51. Morgan, C.L., D.J. Newman, and C.P. Price, Immunosensors: Technology and opportunities in laboratory medicine. Clinical Chemistry, 1996. 42(2): p. 193-209.
52. Wang, J., Towards genoelectronics: Electrochemical biosensing of DNA hybridization. Chemistry-a European Journal, 1999. 5(6): p. 1681-1685.
53. Xiao, Y., et al., Single-step electronic detection of femtomolar DNA by target-induced strand displacement in an electrode-bound duplex. Proceedings of the National Academy of Sciences of the United States of America, 2006. 103(45): p. 16677-16680.

54. Stern, E., et al., Label-free immunodetection with CMOS-compatible semiconducting nanowires. Nature, 2007. 445(7127): p. 519-522.
55. Sheehan, P.E. and L.J. Whitman, Detection limits for nanoscale biosensors. Nano Letters, 2005. 5(4): p. 803-807.
56. Squires, T.M., R.J. Messinger, and S.R. Manalis, Making it stick: convection, reaction and diffusion in surface-based biosensors. Nature Biotechnology, 2008. 26(4): p. 417-426.
57. Nair, P.R. and M.A. Alam, Performance limits of nanobiosensors. Applied Physics Letters, 2006. 88(23): p. -.
58. Jonghyun Go, M.A.A., Statistical Interpretation of Femto-Molar Detection, in Biological Physics. 2009.
59. Decuzzi, P., et al., A theoretical model for the margination of particles within blood vessels. Annals of Biomedical Engineering, 2005. 33(2): p. 179-190.
60. Decuzzi, P. and M. Ferrari, Design maps for nanoparticles targeting the diseased microvasculature. Biomaterials, 2008. 29(3): p. 377-384.
61. Pierres, A., et al., Diffusion of microspheres in shear flow near a wall: Use to measure binding rates between attached molecules. Biophysical Journal, 2001. 81(1): p. 25-42.
62. Decuzzi, P. and M. Ferrari, The adhesive strength of non-spherical particles mediated by specific interactions. Biomaterials, 2006. 27(30): p. 5307-14.
63. Decuzzi, P., et al., Adhesion of microfabricated particles on vascular endothelium: A parametric analysis. Annals of Biomedical Engineering, 2004. 32(6): p. 793-802.
64. Zhang, L., et al., Immersed finite element method. Computer Methods in Applied Mechanics and Engineering, 2004. 193(21-22): p. 2051-2067.
65. Liu, W.K., et al., Immersed finite element method and its applications to biological systems. Computer Methods in Applied Mechanics and Engineering, 2006. 195(13-16): p. 1722-1749.
66. Lawrence, M.B. and T.A. Springer, Leukocytes Roll on a Selectin at Physiological Flow-Rates - Distinction from and Prerequisite for Adhesion through Integrins. Cell, 1991. 65(5): p. 859-873.
67. Bell, G.I., M. Dembo, and P. Bongrand, Cell-Adhesion - Competition between Nonspecific Repulsion and Specific Bonding. Biophysical Journal, 1984. 45(6): p. 1051-1064.
68. Bell, G.I., Models for Specific Adhesion of Cells to Cells. Science, 1978. 200(4342): p. 618-627.
69. Dong, C. and X.X. Lei, Biomechanics of cell rolling: shear flow, cell-surface adhesion, and cell deformability. Journal of Biomechanics, 2000. 33(1): p. 35-43.
70. Chang, K.C., D.F.J. Tees, and D.A. Hammer, The state diagram for cell adhesion under flow: Leukocyte rolling and firm adhesion. Proceedings of the National Academy of Sciences of the United States of America, 2000. 97(21): p. 11262-11267.
71. Einstein, A., Investigations on the Theory of Brownian Movement. 1956: New York: Dover.
72. Ermak, D.L. and J.A. Mccammon, Brownian Dynamics with Hydrodynamic Interactions. Journal of Chemical Physics, 1978. 69(4): p. 1352-1360.

73. Li, A. and G. Ahmadi, Dispersion and Deposition of Spherical-Particles from Point Sources in a Turbulent Channel Flow. Aerosol Science and Technology, 1992. 16(4): p. 209-226.
74. Mody, N.A. and M.R. King, Influence of Brownian motion on blood platelet flow behavior and adhesive dynamics near a planar wall. Langmuir, 2007. 23(11): p. 6321-8.
75. Longest, P.W. and C. Kleinstreuer, Comparison of blood particle deposition models for non-parallel flow domains. Journal of Biomechanics, 2003. 36(3): p. 421-430.
76. Gentile, F., M. Ferrari, and P. Decuzzi, The transport of nanoparticles in blood vessels: The effect of vessel permeability and blood rheology. Annals of Biomedical Engineering, 2008. 36(2): p. 254-261.
77. Sharma, N. and N.A. Patankar, Direct numerical simulation of the Brownian motion of particles by using fluctuating hydrodynamic equations. Journal of Computational Physics, 2004. 201(2): p. 466-486.
78. Mori, N., M. Kumagae, and K. Nakamura, Brownian dynamics simulation for suspensions of oblong-particles under shear flow. Rheologica Acta, 1998. 37(2): p. 151-157.
79. Inthavong, K., et al., Numerical study of fibre deposition in a human nasal cavity. Journal of Aerosol Science, 2008. 39(3): p. 253-265.
80. Haider, A. and O. Levenspiel, Drag Coefficient and Terminal Velocity of Spherical and Nonspherical Particles. Powder Technology, 1989. 58(1): p. 63-70.
81. Tran-Cong, S., M. Gay, and E.E. Michaelides, Drag coefficients of irregularly shaped particles. Powder Technology, 2004. 139(1): p. 21-32.
82. Saad, Y. and M.H. Schultz, Gmres - a Generalized Minimal Residual Algorithm for Solving Nonsymmetric Linear-Systems. Siam Journal on Scientific and Statistical Computing, 1986. 7(3): p. 856-869.
83. McQuarrie, D.A., Kinetics of Small Systems I. Journal of Chemical Physics, 1963. 38(2): p. 433-436.
84. Decuzzi, P. and M. Ferrari, The adhesive strength of non-spherical particles mediated by specific interactions. Biomaterials, 2006. 27(30): p. 5307-5314.
85. Gao, J., unpublished data. Red star is micelles of 100 nm in diameter trapped in tumor. 2008.
86. Muzkantov, ISI adhesion in lung, red star for 1 μm diameter spheres and pink star for 0.1 μm ×1μm×3 μm disks (ten times higher specificity in lung). 2008.
87. Haynes, R.H. and A.C. Burton, Role of the non-Newtonian behavior of blood in hemodynamics. Am J Physiol, 1959. 197: p. 943-50.
88. Bugliarello, G. and J. Sevilla, Velocity distribution and other characteristics of steady and pulsatile blood flow in fine glass tubes. Biorheology, 1970. 7(2): p. 85-107.
89. Srivastava, V.P., A Theoretical Model for Blood Flow in Small Vessels. Applications and Applied Mathematics, 2007. 2(1): p. 51-65.
90. Sharan, M. and A.S. Popel, A two-phase model for flow of blood in narrow tubes with increased effective viscosity near the wall. Biorheology, 2001. 38(5-6): p. 415-28.

91. Nair, P.K., J.D. Hellums, and J.S. Olson, Prediction of oxygen transport rates in blood flowing in large capillaries. Microvasc Res, 1989. 38(3): p. 269-85.
92. Pralhad, R.N. and D.H. Schultz, Two-layered blood flow in stenosed tubes for different diseases. Biorheology, 1988. 25(5): p. 715-26.
93. Woodcock, J.P., Physical-Properties of Blood and Their Influence on Blood-Flow Measurement. Reports on Progress in Physics, 1976. 39(1): p. 65-127.
94. Bayliss, L.E., The axial drift of the red cells when blood flows in a narrow tube. J Physiol, 1959. 149: p. 593-613.
95. Taylor, M., The flow of blood in narrow tubes. II. The axial stream and its formation, as determined by changes in optical density. Aust J Exp Biol Med Sci, 1955. 33(1): p. 1-15.
96. Lutters, B.C., et al., Blocking endothelial adhesion molecules: a potential therapeutic strategy to combat atherogenesis. Curr Opin Lipidol, 2004. 15(5): p. 545-52.
97. Sakhalkar, H.S., et al., Leukocyte-inspired biodegradable particles that selectively and avidly adhere to inflamed endothelium in vitro and in vivo. Proc Natl Acad Sci U S A, 2003. 100(26): p. 15895-900.
98. Sakhalkar, H.S., et al., Enhanced adhesion of ligand-conjugated biodegradable particles to colitic venules. Faseb J, 2005. 19(7): p. 792-4.
99. Zou, X., et al., PSGL-1 derived from human neutrophils is a high-efficiency ligand for endothelium-expressed E-selectin under flow. Am J Physiol Cell Physiol, 2005. 289(2): p. C415-24.
100. Yogeswaran, U. and S.M. Chen, A review on the electrochemical sensors and biosensors composed of nanowires as sensing material. Sensors, 2008. 8(1): p. 290-313.
101. Daniels, J.S. and N. Pourmand, Label-free impedance biosensors: Opportunities and challenges. Electroanalysis, 2007. 19(12): p. 1239-1257.
102. Vijayendran, R.A., F.S. Ligler, and D.E. Leckband, A computational reaction-diffusion model for the analysis of transport-limited kinetics. Analytical Chemistry, 1999. 71(23): p. 5405-5412.
103. Gao, Z.Q., et al., Silicon nanowire arrays for label-free detection of DNA. Analytical Chemistry, 2007. 79(9): p. 3291-3297.
104. Wang, J., Electrochemical biosensors: Towards point-of-care cancer diagnostics. Biosensors & Bioelectronics, 2006. 21(10): p. 1887-1892.
105. Hammer, D.A. and S.M. Apte, Simulation of Cell Rolling and Adhesion on Surfaces in Shear-Flow - General Results and Analysis of Selectin-Mediated Neutrophil Adhesion. Biophysical Journal, 1992. 63(1): p. 35-57.
106. Chang, K.C. and D.A. Hammer, Influence of direction and type of applied force on the detachment of macromolecularly-bound particles from surfaces. Langmuir, 1996. 12(9): p. 2271-2282.
107. Smith, D.E. and C.B. Harris, Generalized Brownian Dynamics .1. Numerical-Integration of the Generalized Langevin Equation through Autoregressive Modeling of the Memory Function. Journal of Chemical Physics, 1990. 92(2): p. 1304-1311.
108. Russel, W.B., Saville, D.A., Schowalter, W.R., Colloidal Dispersions. 1989: Cambridge University Press.

109. Ghosal, S., Fluid mechanics of electroosmotic flow and its effect on band broadening in capillary electrophoresis. Electrophoresis, 2004. 25(2): p. 214-28.
110. de la Rica, R., C. Fernandez-Sanchez, and A. Baldi, Electric preconcentration and detection of latex beads with interdigitated electrodes. Applied Physics Letters, 2007. 90(17): p. -.
111. Gray, D.S., et al., Dielectrophoretic registration of living cells to a microelectrode array (vol 19, pg 1765, 2004). Biosensors & Bioelectronics, 2004. 19(12): p. 1765-1774.
112. Yang, M., et al., A novel microfluidic impedance assay for monitoring endothelin-induced cardiomyocyte hypertrophy. Biosensors & Bioelectronics, 2007. 22(8): p. 1688-1693.

## BIOGRAPHICAL INFORMATION

Samar Shah graduated with a Bachelor of Engineering degree in Mechanical Engineering from Sardar Patel University, India in June 2006. After completing his Bachelor's, he worked as a management trainee at Atul Limited (India) from July 2006 to July 2007. He began his Master's program in Mechanical Engineering at University of Texas at Arlington from August 2007. Soon he joined Dr. Liu's Bionanofluidics lab and worked on research projects, mainly dealing with multiscale modeling of biological systems.

Samar Shah received his master's degree in mechanical engineering from the University of Texas at Arlington in August 2009.